5-2013

Effects Of Stream Restoration And Storm Events On Stream-Groundwater Interactions

Margaret Zimmer
Syracuse University

Abstract

The body of literature on stream-groundwater interactions is rapidly growing, but little is known about the effects of either storm events or in-stream restoration on the interactions between surface water and groundwater. The chapters of this thesis explore two of these questions at the same locality of interest: (1) subsurface geochemical dynamics across a riffle bedform in an unrestored stream during a storm event and subsurface geochemical, and (2) hyporheic exchange dynamics at baseflow conditions pre- and one year post- stream restoration.

The study site was a 30 m stretch of stream that underwent stream restoration through installation of a cross-vane and engineered rock riffle over a natural pool-riffle-pool sequence. Pre-restoration, mini-piezometers and temperature profile rods were spatially located around the riffle. Fourteen mini-piezometers were installed at a 15 cm depth into the streambed and coupled with temperature profile rods that recorded temperature in the water column as well as at 5 cm intervals to a depth of 30 cm into the streambed. Sampling of pore water occurred during baseflow conditions as well as during and after Tropical Storm Irene. Principal component analysis was used to understand the controls on both spatial and temporal stream and pore water chemistry. Through the use of a MATLAB program that utilizes a one-dimensional heat transport model, vertical exchange rates in the streambed were calculated using the measured temperature fluctuations in the streambed during baseflow conditions. Similar to pre-restoration, 19 mini-piezometers and 10 temperature profile rods recorded pore water geochemistry and vertical exchange rates around the installed cross-vane and engineered rock riffle during baseflow conditions one year after restoration.

Pre-restoration, the majority of spatial variability in pore water geochemistry (62%) is driven by differential mixing of surface and ground water across the hyporheic zone. The second largest driver of pore water geochemistry (17%) was temporal dilution and re-enrichment of

infiltrating surface water during Tropical Storm Irene. Hyporheic sites minimally affected by upwelling groundwater showed temporal fluctuations in pore water geochemistry across the reach influenced by both changes in infiltrating stream chemistry as well as hyporheic residence time and flowpath length. The streambed zone influenced by groundwater discharge increased in size during Tropical Storm Irene, indicating that the area of localized groundwater inputs grows in response to storm events.

After restoration, hyporheic exchange rates increased by an order of magnitude immediately adjacent to the cross-vane and engineered rock riffle, when compared to exchange rates around the riffle in pre-restoration conditions. Away from the restoration structure, exchange rates are similar between pre- and post- restoration. A Rhodamine WT injection suggested 100% of streambed pore water immediately adjacent to the structure originated from the stream, while the rest of the study site received roughly 20 percent stream water. Evidence of nitrate production and uptake were seen across the pre-restoration riffle, but the post-restoration cross-vane and rock riffle showed evidence of only nitrate uptake. Therefore, although restoration produces hot spots of hyporheic exchange, the high exchange rates reduce hyporheic flow path residence time such that nitrate production cannot change nitrate concentrations in the streambed. While zones of groundwater inputs are present pre- and post- restoration, the zone of groundwater upwelling increased post-restoration, suggesting cross-vane installation may have disturbed subsurface hydraulic conductivity.

EFFECTS OF STREAM RESTORATION AND STORM EVENTS ON STREAM-GROUND WATER INTERACTIONS

By

Margaret Ann Zimmer
B.A. Environmental Studies, Oberlin College, 2011

Thesis

Submitted in partial fulfillment of the requirements for the degree of
Master of Science in Earth Sciences.

Syracuse University

May 2013

Acknowledgements

I would like to thank my MS advisor, Dr. Laura Lautz, for the effort and dedication she put into my education and research. Dr. Lautz gave me the flexibility, financial support, and diligent professional and research guidance to ensure I reached all my graduate school goals. Words could never express how grateful I am for my time learning from Dr. Lautz. I am forever indebted to Drs. Scott Bailey and Kevin McGuire for teaching me to question and be confident, and for introducing me to the truly exciting world of hydrology. I would like to thank my research group and fellow graduate students for all the great experiences. Finally, I would like to thank my family and friends for enduring my ramblings and constantly supporting me through each new project and obsession as well as to Steve for braving a run in with poison ivy in the name of science.

Table of Contents

Abstract i

Acknowledgements v

Table of Contents vi

Temporal and spatial response of hyporheic zone geochemistry to a storm event

1. Introduction **1**

2. Methods **5**

2.1 Site description 5

2.2 Precipitation and hydrograph information 5

2.3 Streambed instrumentation and storm sampling 6

2.4 Multivariate statistical analysis 8

3. Results **9**

3.1 Principal component analysis: All sites 9

3.2 Principal component analysis: Surface water rich sites 11

3.3 Streambed chemistry in lagged and well-connected sites 12

3.4 Baseflow stream and streambed geochemistry 13

3.5 Storm event stream and streambed geochemistry 14

3.6 Chemical variability versus depth of sampling 15

4. Discussion **16**

4.1 Source delineation 16

4.2 Event response 17

4.3 Conceptual model 22

5. Conclusions **25**

Tables **28**

Figures **31**

Appendix **40**

Pre- and post- restoration assessment of stream-ground water interactions: impacts on hydrological and chemical heterogeneity in the hyporheic zone

1. Introduction **42**

2. Methods **46**

2.1 Site Description 46

2.2 Stream instrumentation and sampling 46

3. Results **49**

3.1 Streambed morphology: pre and post- restoration 49

3.2 Baseflow geochemistry and vertical exchange rates 50

3.2.1 Pre-restoration 50

3.2.2 Post-restoration 52

3.3 Percent stream water in streambed: post-restoration 53

4. Discussion **54**

4.1 Zones of upwelling and downwelling pre- and post- restoration 54

4.2 Biogeochemical differences pre- and post- restoation 56

4.3 Ecological Implications 58

5. Conclusions **62**

Tables **64**

Figures **65**

References Cited **73**

Vita 86

List of Tables

Table 1.1 Principal Component Analysis 1 Parameters.....28

Table 1.2 Principal Component Analysis 2 Parameters 29

Table 1.3 Pore Water Chemistry.....30

Table 2.1 Stream and Pore Water Chemistry.....64

List of Figures

Figure 1.1 Site Map 31
Figure 1.2 Principal Component Analysis 1 32
Figure 1.3 Vertical Exchange Rates 33
Figure 1.4 Principal Component Analysis 2 34
Figure 1.5 Spatial Chemistry 35
Figure 1.6 Chemistry Time Series 36
Figure 1.7 Chemistry Time Series 37
Figure 1.8 Chemistry By Depth 38
Figure 1.9 Spatial Principal Component 39

Figure 2.1 Site Map 65
Figure 2.2 Streambed Topography 66
Figure 2.3 Bivariate Chemistry 67
Figure 2.4 Spatial Chemistry 68
Figure 2.5 Nitrate and Dissolved Oxygen 69
Figure 2.6 Vertical Exchange Rates 70
Figure 2.7 Vertical Exchange Rates 71
Figure 2.8 Percent Stream Water 72

Chapter 1. Temporal and spatial response of hyporheic zone geochemistry to a storm event

(Note: This manuscript is published in the journal, Hydrological Processes)

1. Introduction

The hyporheic zone marks the dynamic ecotone where stream water interacts with the surrounding subsurface aquifer, allowing for mixing with groundwater (Hayashi and Rosenberry, 2002). Hyporheic exchange is the process by which water from the stream infiltrates into the hyporheic zone, either in the streambed or adjacent stream banks, and returns to the stream over small distances or time (Harvey *et al.,* 1996; Gooseff, 2010). Hyporheic exchange, which is influenced by stream discharge, hydraulic conductivity, and channel morphology (Wroblicky *et al.,* 1998; Harvey and Wagner, 2000; Storey *et al.,* 2003), can transport, retain and transform nutrients and oxygen while providing for unique benthic and riparian habitats (Boulton *et al.,* 1998).

Recent model and field experiments on stream-groundwater interactions have focused largely on understanding how bedform topography produces predictable zones of hyporheic exchange during steady-state conditions (e.g. Kasahara and Wondzell, 2003; Kasahara and Hill, 2006; Cardenas and Wilson, 2007; Fanelli and Lautz, 2008; Hester and Doyle, 2008; Wondzell, 2011; Briggs *et al.,* 2012). Kasahara and Hill (2006) showed that during baseflow conditions in riffle bedforms there are zones of surface water downwelling immediately upstream of riffle bedforms, which produce oxic streambed conditions. They showed zones of groundwater upwelling occur immediately downstream of riffle bedforms, which produce anoxic streambed conditions. This predictable spatial patchiness drives the development of micro-environments throughout the streambed, by providing variable amounts of dissolved oxygen, nutrients and organic matter across the system (Valett *et al.,* 1994; Hayashi and Rosenberry, 2002; Boulton,

2007). However, it is unclear how this spatial patchiness around riffle bedforms persists during, or responds to, periods of non-baseflow conditions.

Most annual watershed export of solutes occurs during storms (Hornberger *et al.,* 1994; Creed and Band, 1998). However, the geochemical role and response of the hyporheic zone to storms is currently poorly understood (Wondzell, 2011). Based on a literature review described in the following paragraphs, there are currently two main physical processes thought to control hyporheic exchange during periods of fluctuating stream stage, such as storms. The first process is the increase in hydraulic head at the streambed interface as stream stage increases, which causes a rapid influx of stream water into the hyporheic zone. The second process is the increase in the hydraulic gradient toward the stream, resulting from storm water recharge to the adjacent groundwater aquifer, which causes the size of the hyporheic zone to decrease.

The majority of studies that have investigated the increase in hyporheic exchange in response to rising stream stage (i.e. the first process described above) are field studies that focus on measurements within the stream channel at relatively shallow depths, have no precipitation input, and largely ignore adjacent aquifer dynamics (e.g. D'Angelo *et al.,* 1993; Arntzen *et al.,* 2006; Sawyer *et al.,* 2009; Briggs *et al.,* 2012). Gerecht *et al.* (2011) showed that hyporheic exchange went from upwelling to downwelling with an increase in stream stage during a dam storage-release cycle. Similarly, Fritz and Arntzen (2007) and Francis *et al.* (2010) saw a positive correlation between artificial fluctuations in stream stage and hyporheic exchange in field studies around regulated dam spillways. Further, some modeling studies that focused analysis on the stream and ignored groundwater upwelling (Boano *et al.,* 2007; Boano *et al.,* 2010) showed an increase in exchange rates with increasing stream stage.

Studies that have investigated the decrease in hyporheic zone size during storm events (i.e. the second process described above) are primarily modeling studies that take into account groundwater dynamics in the surrounding aquifer (e.g. Harvey and Bencala, 1993; Wroblicky *et al.*, 1998; Storey *et al.*, 2003). Wondzell and Swanson (1996) used a MODFLOW model to show that subsurface flow rates to a gravel bar adjacent to a 4th order stream positively correlate to stream discharge during baseflow conditions, but decrease during storm events due to precipitation inputs to the aquifer. Shibata *et al.* (2004) also used MODFLOW to demonstrate that contributions of soil water to the stream from the adjacent hillslope increase during storm events, while stream water contributions to the adjacent aquifer decrease. Boano *et al.* (2008) modeled that an increase in groundwater levels in the adjacent aquifer altered hyporheic exchange rates across the stream channel differently, based on lateral distance from the aquifer. They showed exchange rates were reduced along the banks and the majority of hyporheic exchange was confined to the central part of the stream, where upwelling groundwater flowpaths from the adjacent aquifer were not as influential.

Some studies that have used both streambed and adjacent aquifer analyses to investigate hyporheic response to changing stream stage have shown the influence of both processes during storm events. A field study by Morrice *et al.* (1997) showed that a seasonal increase in stream discharge and hydraulic gradients toward the stream from a seasonal rise in the water table, increased the rate of hyporheic exchange, but reduced the size of the hyporheic zone. Similarly, Hart *et al.* (1999) showed in a field study that storage zone size did not change in response to variations in flow conditions, but rates of exchange increased due to increasing stream discharge. Malcolm *et al.* (2004) saw in a field study that on a weekly scale, low flow conditions promoted groundwater contributions to the hyporheic zone and higher flow conditions promoted increased

surface water contributions to the hyporheic zone. Malcolm *et al*. (2004) further showed that during storm events, high-resolution hydraulic head data in the center of a riffle bedform indicated that the stream went from slightly gaining to losing during the rising limb of storm hydrographs. Upward gradients were re-established late into the receding limb of the storm hydrograph. Westhoff *et al.* (2011) examined groundwater and stream water inputs throughout the hyporheic zone during a small precipitation event and saw an increase in stream water infiltration to the streambed, but no change in groundwater inputs.

The majority of field studies on hyporheic zone response to variable stream discharge examine how hyporheic exchange responds to seasonal changes in stream stage (e.g. Wondzell and Swanson, 1996; Morrice *et al.,* 1997; Hart *et al.,* 1999; Malcolm *et al.,* 2004; Briggs *et al.,* 2012) or dam-regulated stream flow (e.g. Fritz and Arntzen, 2007; Francis *et al.,* 2010, Gerecht *et al.,* 2011), or how hyporheic exchange varies between streams with different magnitudes of discharge (e.g. D'Angelo *et al*., 1993). Fewer studies examine hyporheic exchange responses to storm events (e.g. Wondzell and Swanson, 1996; Malcolm *et al.,* 2004; 2006), however most of these studies predominantly focus on physical hydrology and not geochemical changes. Our study addresses the gap in knowledge regarding how stream-groundwater exchange rates and streambed geochemistry respond to a rapid fluctuation in stream stage, such as during a large scale storm event. To address this gap in knowledge, we measured spatial and temporal changes in surface water and pore water solute concentrations in a 40 m reach of a stream during a large storm event, specifically Tropical Storm Irene in August 2011. The objectives of this study were to (1) characterize spatial vertical water exchange rates and geochemical patterns in the hyporheic zone around a pool-riffle-pool bedform during baseflow, and (2) use results from

principal component analyses and time-series geochemical analyses to conceptualize how different regions of the hyporheic zone respond to storm events.

2. Methods

2.1 Site Description

This study was conducted along a 40 m stream reach of Chittenango Creek (Figure 1.1), an ungauged tributary to Oneida Lake, near Syracuse, New York, USA (43°00' 32.27" N 75°50' 49.85" W, elevation ~178 m). The drainage area to Chittenango Creek is 750 km^2. The study reach parallels State Highway 13 and is downstream of Chittenango Falls, a 51 m waterfall. The study reach is a pool-riffle-pool sequence and the streambed is comprised of coarse sand and gravel. An acoustic doppler velocimeter measurement of discharge calculated 0.80 m^3s^{-1} at the study reach during the August baseflow survey.

2.2 Precipitation and Hydrograph Information

The recurrence interval of Tropical Storm Irene at our study site was a 2 to 5 year storm, as interpreted by data provided by Northeast Regional Climate Center and Natural Resources Conservation Service (http://precip.eas.cornell.edu). Due to the short range forecast limiting preparation time, as well as safety considerations of collecting data during Tropical Storm Irene, precipitation and stream discharge measurements from National Oceanic and Atmospheric Administration (NOAA) and United States Geological Survey (USGS) stations in central New York were used as a proxy for the conditions at our specific site. Daily precipitation data used for this study were collected in the town of Chittenango (Station ID: US1NYMD0016) by the National Climatic Data Center within NOAA. Approximately 6.2 cm of precipitation were

measured at this station during the storm. Hydrographs were created from hourly discharge measurements taken at several regional USGS Stations, all less than 55 kilometers from the study site, including: Oneida Creek at Oneida, NY (04243500), East Branch Fish Creek at Taberg, NY (04242500), and Otselic River at Cincinnatus, NY (01510000). We chose these three sites as they were geographically close to the study site and were relatively similar, albeit smaller, in contributing area. Discharge at each site was normalized to the highest discharge value during the study period in order to compare timing of peak discharge and storm flow recession. The discharge at the end of the study period was, on average, 25% greater than pre-event discharge at the three gauging stations.

2.3 Streambed Instrumentation and Storm Sampling

To evaluate the topographic controls on stream and streambed interaction, we surveyed the morphology of the study site with a Nikon Nivo 5.M total station, which has a spatial resolution of <1 cm. We collected spatial information at 167 survey points to characterize bedform morphology, water elevation, water edge, and position of installed sampling equipment during baseflow conditions (Figure 1.1).

Temperature profile rods were coupled with mini-piezometers at 14 locations across the 40 m stream reach (Figure 1). Temperature profile rods contained seven vertically-stacked temperature sensors (iButton DS1922L, Maxim Integrated, San Jose, CA), with six installed in the streambed at 5-cm intervals to a depth of 30 cm and one positioned in the water column (depth = 0 cm). The temperature sensors recorded temperature at 10-minute intervals for seven days prior to the storm. Vertical water exchange rates at each location were calculated for baseflow conditions prior to the storm event using one-dimensional heat transport modeling

(Hatch *et al.*, 2006; Gordon *et al.*, 2012). We used VFLUX (Gordon *et al.*, 2012), a MATLAB computer program, which derives exchange rates every two hours during the observation period from the difference in amplitude of the propagated diurnal temperature signal measured at multiple depths (Hatch *et al.*, 2006). Exchange rates were calculated at depths of 2.5 cm and 5.0 cm using the 0-5 cm and 0-10 cm pairs of sensors, respectively. Two-hour exchange rates at both depths were averaged over the 7-day baseflow observation period to derive a single vertical exchange rate across the streambed interface for each observation point.

Mini-piezometers were constructed of PVC pipe (1.27 cm ID) with a 5 cm screen created by drilling a series of 0.3 cm diameter holes in the pipe. These mini-piezometers were installed 17.5 cm below the stream-streambed interface, such that the 5 cm screen was centered at 15 cm. Plastic tubing and a syringe were used to purge and sample pore water from the piezometers. At four of the 14 mini-piezometer locations (P02, P05, P07, P11), we installed nested piezometers to determine how bed chemistry varies with streambed depth. At P02 and P11, we installed mini-piezometers at 32.5 cm in addition to the standard depth of 17.5 cm. At P05 and P07, we installed mini-piezometers at 27.5 and 32.5 cm in addition to the standard depth of 17.5 cm.

Stream water as well as pore water from the mini-piezometers was sampled seven times throughout the study period. Of the seven sampling times, one baseflow sampling occurred on 27 August 2011, one sampling occurred during the rising limb of Tropical Storm Irene on 28 August 2011, and five samplings occurred once daily during the receding limb of the storm hydrograph from 30 August to 3 September 2011. There is a two day gap of no sampling during the peak portion of the stream hydrograph (28 and 29 August 2011) due to high flows limiting safe accessibility to the stream and sampling locations.

Samples were collected within a two-hour period on each sample date and were filtered with a 0.7 µM glass microfiber filter within an eight-hour period. Specific conductance (SC), pH and dissolved oxygen (DO) were measured in the field. Dissolved metals, specifically calcium (Ca^{2+}), sodium (Na^{+}), magnesium (Mg^{2+}), ammonium (NH_4^{+}), and potassium (K^{+}), as well as anions, specifically fluoride (F^{-}), bromide (Br^{-}), phosphate (PO_4^{2-}), chloride (Cl^{-}), nitrate (NO_3^{-}) and sulfate (SO_4^{2-}) were analyzed on a Dionex ICS-2000 Ion Chromatograph. For this study, NH_4^{+}, Br^{-}, and PO_4^{2-} were not used because most samples registered below the detection limit.

2.4 Multivariate Statistical Analysis

Principal component analysis (PCA) is a statistical tool used to summarize covariance between variables in large datasets by creating linear combinations of the original variables. Several recent studies have used PCA to summarize the variability of stream-groundwater interactions (Lautz and Fanelli, 2008; Lewandowski *et al.*, 2009; Guggenmos *et al.*, 2011).

In our study, we used the PRINCOMP method in the computer program MATLAB to run a PCA to interpret the relationships between solutes across the entire spatial and temporal stream and streambed geochemical dataset. Before the PCA, we standardized the variables by subtracting the mean value for each solute and dividing by the standard deviation for each solute. By normalizing the dataset, we removed the weighted influence of different solutes based on their relative concentrations. We then transformed our nine standardized input variables, HCO_3^{-}, F^{-}, Cl^{-}, NO_3^{-}, SO_4^{2-}, Na^{+}, K^{+}, Mg^{2+}, and Ca^{2+}, into nine linear combinations, or PC scores. The coefficients, or loadings, for each variable represent the relative importance of each individual variable for computing the PC scores and are used to interpret the meaning of the PCs. The variance summarized by each PC can be expressed as a percentage of the total data variance.

We initially ran a PCA with the complete geochemistry dataset (PC1) and subsequently used those results to identify GW-rich versus SW-rich sites in the streambed. We then ran a second PCA on the SW-rich sites (PC2) to more clearly identify controls on stream and streambed geochemistry during the storm event. The first PCA focused on spatial variability within the geochemical dataset and the second PCA focused on temporal variability within the geochemical dataset. Further details on site categorization, as well as the results from both PCAs are described in Results Sections 3.1 and 3.2.

3. Results

3.1 Principal Component Analysis: All Sites

Principal component analysis of all stream and streambed water samples (PC1, n=111) collected during the sampling period showed how solute concentrations in the stream and streambed co-varied in both space and time (Table 1.1 and Figure 1.2). This analysis yielded nine linear combinations (principal components, PC), however, only the first two PCs were used in this study. These two PCs accounted for 79% of the variance within the dataset. The first principal component (PC1.1) accounted for 62% of the variance within the complete dataset and is positively correlated with Ca^{2+}, Mg^{2+}, and SO_4^{2-}, and negatively correlated with Na^{+} and Cl^{-} (Table 1.1). PC1.1 is referred to as the "GW-influence" function, as it represents the spatial influence of relatively $Ca^{2+}/Mg^{2+}/SO_4^{2+}$-poor, Na^{+}/Cl^{-}-rich surface water and relatively $Ca^{2+}/Mg^{2+}/SO_4^{2-}$-rich, Na^{+}/Cl^{-}-poor groundwater at each streambed site. This "GW-influence" function primarily captures spatial differences between sites that have variable contributions of groundwater. Low scores for PC1.1 (<0) indicate sites primarily comprised of stream water. Stream water samples had negative PC1.1 scores between -1.8 and -0.8. Streambed sites that stay

below or at zero are thus considered SW-rich and are designated with green and red points in Figure 1.2. Positive scores for PC1.1 (>0) indicate hyporheic sites strongly influenced by mixing with groundwater (Figure 1.2). These sites (P01, P02, P05 and P09) are considered to be GW-rich sites, which are designated with black points in Figure 2. Heat transport modeling results of vertical water exchange show these sites are upwelling, with an average exchange rate of -16 cm/d, during baseflow conditions (Figure 1.3). P03 is the only transitional site between the SW-rich and GW-rich categories, which is designated with grey points on Figure 1.2. While P03 started as a SW-rich site during baseflow conditions, it showed a larger change in PC1.1 scores than the stream and any other SW-rich site during the storm (Figure 1.2). This large change in GW-influence score suggests that discharge of GW to P03 increased during the storm.

The second principal component (PC1.2) accounted for 17% of the variance within the dataset and is most strongly correlated with concentrations of Na^+, Cl^-, and HCO_3^- (Table 1.1). PC1.2 was primarily used to summarize temporal variations in geochemistry at individual sites during the storm event. The loadings for all solutes for PC1.2 were positive, indicating that all solute concentrations are relatively enriched in samples with high PC1.2 scores (>0) and solute concentrations are relatively dilute when the PC1.2 score is low (<0). PC1.2 is therefore referred to as the "storm dilution" function, as it represents the dilution of solutes during the storm event, and the subsequent re-enrichment as the system rebounds from the storm event.

All streambed pore water and stream water samples initially had storm dilution scores greater than zero, indicating relative enrichment of all ion concentrations before the storm event. The storm dilution score for stream water dropped from 0.4 to -1.6 during the storm, reflecting the dilution of all ions during the event, and rebounded to a value of -0.4 following the event, showing re-enrichment of ions (Figure 1.2). All streambed pore water showed some degree of

overall solute dilution during the storm event that mirrored the stream water response, as indicated by a decrease in the storm dilution score at all sites during the event. However, the GW-rich sites showed a notably smaller dilution response than SW-rich sites (Figure 1.2) and the majority of GW-rich samples did not dip below zero for PC1.2. While none of the GW-rich sites dipped below the lowest PC1.2 score within the SW samples (-1.6), many SW-rich sites dipped well below that value, with a minimum PC1.2 score of -3.4 for site P12.

3.2 Principal Component Analysis: Surface Water Rich Sites

The first principal component analysis (PC1) indicates that the majority (62%) of the variance in the complete dataset is associated with the varying spatial influence of GW at the various sites (PC1.1). To tease out temporal relationships associated with the storm event, we removed the GW-rich sites (P01, P02, P05 and P09) as well as transitional site P03 from the dataset for our second principal component analysis (PC2, n=77). By subsetting the dataset in this way, we were able to minimize GW influence and isolate streambed pore water samples that were primarily influenced by stream water infiltration. This allowed us to more closely scrutinize the temporal variability of pore water chemistry at these connected streambed sites during the storm event.

The PC2 analysis yielded two main PCs that accounted for 72% of the variance within the select dataset (Table 1.2; Figure 1.4). The first PC (PC2.1) accounted for 54% of the variance within the dataset and is similar to PC1.2 in that it is strongly correlated with Na^+, Cl^-, HCO_3^-, and has positive loadings for all solutes (Table 1.2). PC2.1 is therefore referred to as another "storm dilution" function, as it represents the flushing of streambed sites by dilute event water, and the subsequent re-enrichment of solute concentrations as the system rebounds from the storm

event. The second PC (PC2.2) accounted for 18% of the variance within the dataset and is most strongly and positively correlated with NO_3^- (Table 1.2). PC2.2 is therefore referred to as the "nitrate" function, as it represents the combined influences of initial enrichment, subsequent dilution, and biogeochemical processing of NO_3^- before and after the storm event (Figure 1.4).

Based on PC2, we were able to categorize the connected streambed sites into two groups: "well-connected sites" and "lagged sites". Although the majority of the variance in the select dataset can be found in the storm dilution component (PC2.1), the nitrate component (PC2.2) was primarily used to differentiate between well-connected and lagged sites (Figure 1.4). Well-connected sites showed mostly positive nitrate scores both pre- and post- event that varied from -0.15 to 2.1. These sites were generally located at the head of the riffle bedform, at sites P04, P06, P07, P08 and P10, where heat transport modeling shows SW was downwelling during baseflow with an average exchange rate of 8.0 cm/d (Figure 1.3). In contrast, lagged sites had a positive nitrate score during baseflow conditions, but became and stayed negative throughout the storm event (Figure 1.4). These sites were generally located at the tail of the riffle bedform, at sites P11, P12, P13, and P14, where heat transport modeling shows streambed water was upwelling during baseflow with an average exchange rate of -13 cm/d (Figure 1.3).

3.3 Streambed Chemistry in Lagged and Well-connected sites

To summarize differences in the biogeochemical response of well-connected versus lagged sites throughout the storm, we conducted two tailed t-tests on biogeochemically reactive solutes, K^+, NO_3^-, and SO_4^{2-}, as well as pH and DO, between the two categories (Table 1.3). We used a p-value of 0.10 as a significance threshold due to the low number of sample points. At baseflow conditions, the biogeochemically reactive solutes (except SO_4^{2-}), pH and DO were

significantly different between well-connected and lagged sites ($p<0.10$). During the rising limb of the storm there were no significant biogeochemical differences between the well-connected and lagged sites. During the first sample period during the receding limb of the hydrograph, all biogeochemically reactive parameters became significantly different, except K^+. During the second, third and fourth sample periods of the receding limb, all biogeochemically reactive parameters were significantly different between the well-connected and lagged sites ($p<0.10$). By the last sampling period, the differences in solute concentrations between the well-connected and lagged sites returned to pre-event conditions (Table 1.3).

3.4 Baseflow Stream and Streambed Geochemistry

Solute concentrations in stream and streambed pore water reflect the patterns summarized using the PCA analysis. All solute concentrations in SW samples taken at both the head and tail of the 40 m study reach were within five percent during each sampling period, indicating the stream water chemistry was spatially uniform across the study reach. During the baseflow survey, SW chemistry was dominated by SO_4^{2-} (74.3 mg/L) and Ca^{2+} (77.5 mg/L) and had an SC value of 540 μS/cm, DO concentration of 12.1 mg/L, NO_3^- concentration of 2.2 mg/L, and Cl^- concentration of 30.1 mg/L.

In the baseflow survey, we saw relatively uniform, SW-rich pore water geochemistry across the riffle bedform at a screened depth centered at 15 cm below the sediment-water interface, with the exception of zones of GW discharge that were spatially oriented toward the head of the riffle and on the outside of the meander (sites P01, P02, P05, and P09; Figure 1.5). These sites are recognized as GW-rich sites in PC1.1. The zones of GW discharge had relatively high concentrations of SO_4^{2-}, Ca^{2+}, and Mg^{2+} (Figure 1.5a for SO_4^{2-}) and low concentrations of

Na^+ and Cl^-, relative to other streambed sites (Figure 1.5b for Cl^-). The GW-rich sites had high SC values ranging from 805 to 1984 μS/cm, whereas the rest of the streambed sites had stream-like SC values from 559 to 629 μS/cm. Concentrations of DO ranged from 0.9 to 2.0 mg/L in the GW-rich sites and ranged from 1.5 to 9.1 mg/L in the rest of the streambed sites (Figure 1.5d).

Streambed pore water geochemistry outside of zones affected by GW discharge showed some spatial organization around the riffle bedform at baseflow conditions. This spatial organization was represented with well-connected and lagged sites in PC2.2. At baseflow, mean concentrations of biogeochemically reactive ions NO_3^- and K^+ as well as pH and DO were significantly different ($p<0.10$) in SW-rich sites above the riffle relative to SW-rich sites below the riffle, with higher NO_3^- at the upstream sites and higher K^+ at the downstream sites (Table 1.3; 1.Figure 5c for NO_3^- and 5d for DO).

3.5 Storm Event Stream and Streambed Geochemistry

Stream water showed an initial increase in SC and concentrations of K^+, HCO_3^-, Na^+ (~10% increase) and NO_3^- (50% increase) during the rising limb of the storm, but a decrease in all solute concentrations (between 7 and 54%) during the first sampling of the storm recession (Figures 6 and 7 for Cl^-, SO_4^{2-} and NO_3^-). As the stream stage receded over the subsequent three sampling dates, the solute concentrations in the stream increased steadily (Figures 1.6 and 1.7). None of the solute concentrations in the stream water completely returned to pre-event baseflow concentrations (except Mg^{2+}) during the sampling period.

Groundwater rich sites (P01, P02, P05, and P09) showed minimal geochemical response during the storm event, relative to the SW-rich sites (Figures 1.2 and 1.6). These sites had the

highest concentrations of Mg^{2+}, Ca^{2+} and SO_4^{2-} in the streambed, which on average increased from baseflow sampling to the final post-event sampling period.

Outside the streambed zone showing influence of GW discharge, the geochemistry at streambed sites reflected the influence of stream water concentration at varying time scales as well as bedform morphology. Sites upstream of the riffle bedform (well-connected sites) generally responded faster to changes in stream water solute concentrations, while downstream sites (lagged sites) showed a delay in response. For instance, concentrations of Cl^-, a conservative solute, were similar between well-connected and lagged sites during baseflow conditions, but became significantly different during the storm (Table 1.3; Figure 1.6). As Figures 6 and 7 demonstrate, well-connected sites followed changes in stream water closely during the receding limb, while lagged sites presented the solute concentrations of SW and well-connected sites from previous sampling periods. Similarly, although the storm onset caused initial uniformity across well-connected and lagged sites, the storm recession yielded spatial differences in non-conservative ion concentrations. For instance, NO_3^-, SO_4^{2-}, and DO concentrations as well as pH were consistently higher in well-connected sites, while K^+ concentrations were consistently higher in lagged sites throughout the receding limb of the storm event (Table 1.3; Figure 1.7 for NO_3^-).

3.6 Chemical variability versus depth of sampling

We installed nested piezometers at select GW-rich, well-connected and lagged sites (P02, P05, P07, P11) to test chemical variability with depth (from 15 to 30 cm). The temporal variability, or range in concentrations of SO_4^{2-}, a GW indicator, was highest at the 15 cm depth at the GW-rich nested sites (P02 and P05), but lowest at the lagged (P11) and well-connected sites

(P07; Figure 1.8). Concentrations of SO_4^{2-} increased with depth at GW-rich sites, but stayed consistent with depth for well-connected and lagged sites (Figure 1.8). The temporal variability, or range in concentrations of NO_3^-, a SW indicator, was greatest at 15 cm for all nested piezometers. With greater depth, the range decreased, except at the well-connected site (P07). Concentrations of NO_3^- decreased with depth at all nested sites, except the well-connected site (Figure 1.8).

4. Discussion

4.1 Source Delineation

At baseflow conditions, streambed sites can be divided into SW-rich versus GW-rich sites based on geochemistry (Figure 1.5). Surface water-rich sites have higher Na^+, Cl^-, NO_3^-, and DO concentrations, while GW-rich sites have higher SC values and Ca^{2+}, Mg^{2+}, and SO_4^{2-} concentrations. This geochemical distinction between SW-rich and GW-rich sites was confirmed by PC1.1 (Figure 1.2). Within the group of SW-rich sites, NO_3^- and DO concentrations and pH values are generally higher in streambed sites upstream of the riffle bedform (well-connected sites) and lower in sites downstream of the riffle bedform (lagged sites; Figure 1.5; column 1 of Table 1.3). Studies have shown similar spatial patterns along riffle-pool bedform morphology during baseflow conditions (e.g. Kasahara and Hill, 2006; Lautz and Fanelli, 2008). Water infiltrates into the streambed upstream of the riffle, moves along a subsurface flowpath and upwells back into the stream downstream of the riffle, with depletion of DO and NO_3^- concentrations and decrease in pH along the flowpath in response to microbial use of solutes as electron acceptors during the oxidation of organic carbon, and thus acidification, in the

streambed. Our calculated vertical exchange rates at baseflow support these patterns as well (Figure 1.3).

The presence of spatially distributed points of anomalous GW inputs (P01, P02, P05 and P09), as opposed to uniform and spatially diffuse GW inputs, has been seen in other studies (e.g. Conant, 2004; Conant *et al.*, 2007; Lautz and Ribaudo, 2012). These anomalous GW inputs may be a result of the local-scale geology, such as zones of high hydraulic conductivity, which allow for high rates of groundwater discharge. This distribution of chemistry from SW and GW contributions at baseflow conditions suggests there are two main physical drivers in hyporheic geochemistry: (1) the bedform morphology, which drives local subsurface flowpaths, around a pool-riffle-pool bedform in our study, and (2) anomalous groundwater discharge points that provide a GW chemical signature to the hyporheic zone, which are located upstream of the riffle and to the outer edge of the meander in our study.

4.2 Event response

Based on our temporal geochemical analysis, it is apparent the dominant driver of hyporheic exchange during the storm event is an increase in stream stage. At the storm onset, a rise in stream stage causes the streambed to be inundated with dilute event water at all SW-rich sites (Figures 1.6 and 1.7; column 2 of Table 1.3). This is seen in PC1.2 and PC2.1 (storm dilution functions), as the streambed sites (well-connected and lagged sites) show dilute pore water chemistry that reflects stream water dilution during the event (Figures 1.2, 1.4, 1.6, and 1.7). Further, biogeochemically reactive solutes K^+ and NO_3^- as well as pH and DO were significantly different between well-connected and lagged sites before the storm, but become more uniform across these sites during the rising limb (Table 1.3). This suggests either the

flowpaths have decreased in residence time from an increase in stream stage, or the streambed has been uniformly inundated by stream water. Analogous hyporheic response to rapidly changing stream stage has been shown in other hyporheic exchange studies; for example, Arntzen *et al*. (2006), Sawyer *et al.* (2009) and Francis *et al.* (2010) all showed through vertical exchange measurements that increases in stream stage, from daily dam regulated flow release, push stream water into the streambed, even in naturally GW gaining systems (Sawyer *et al.,* 2009). Malcolm *et al.* (2004; 2006) also saw an increase in SW contributions in the streambed during periods of higher stream flow during storm events. In this study, GW-rich sites do not show as much chemical change from infiltrating stream water (Figures 1.2 and 1.6), which may be because the large proportion of GW in the streambed pore water at these locations masks the SW signal. The minimal geochemical response at the GW-rich sites we report could also be a product of a sampling period that was too short to detect the full effects of storm water inputs to the aquifer and thus any longer term changes in groundwater chemistry related to the storm event.

Spatial differences in the response of hyporheic exchange during the storm event can be summarized by dividing the SW-rich sites into two groups we called well-connected and lagged sites, which are differentiated by the patterns seen in PC2.2 (nitrate function; Figure 1.4). Throughout the event, well-connected sites show a similar composition to stream chemistry, suggesting rapid hyporheic exchange during the storm (Figures 1.6 and 1.7). Lagged sites generally show similar dilution/enrichment patterns to well-connected sites, but show lower and/or lagged solute concentrations relative to the stream and well-connected sites throughout the event (Figures 1.6 and 1.7; Table 1.3). The distribution of well-connected and lagged sites is tied to the bedform morphology, as well-connected sites fall within and above the riffle, while

lagged sites fall below the riffle bedform. The lagged response in the downstream sites is thus most likely due to the longer subsurface flowpath for these sites, which causes a lagged arrival of dilute event water and enriching post-event water. Thus, while the stream and well-connected sites are concurrently recovering from event dilution and re-enrichment as the storm passes, the lagged sites reflect the stream chemistry in the recent past (e.g. the prior day). We therefore see concentration differences in conservative solutes like Cl^- between well-connected and lagged sites during event dilution and recovery (Figure 1.6).

Concentrations in biogeochemically reactive solutes, K^+ and NO_3^-, stay significantly different between well-connected and lagged sites throughout the entire sampling period, except during initial flushing of the streambed at the storm onset (Table 1.3). We hypothesize this is due to the stream stage rising rapidly during storm onset, pushing stream water into the streambed, temporarily making the streambed chemically uniform at these SW-rich sites. As the stream stage recedes, however, the localized subsurface flowpaths across the riffle dominate the movement of hyporheic zone water, reproducing differences in biogeochemically reactive solutes between the two groups.

The differences in concentrations of biogeochemically reactive K^+ and DO between well-connected and lagged sites become greater from baseflow to the final post-event sampling (Table 1.3). While the differences in NO_3^- concentrations between well-connected and lagged sites did not become greater from baseflow to final post-event sampling, concentrations were relatively low at the lagged sites throughout the receding limb of the storm hydrograph, while connected sites began to recover in NO_3^- concentrations (Figure 1.7; Table 1.3). We hypothesize the spatial difference in these biogeochemically reactive solutes is due to changes in microbial processing along the subsurface flowpaths. Although we did not measure dissolved organic carbon (DOC),

we hypothesize a rapid influx of DOC in the stream during the storm may have occurred, as seen in several studies (Hinton *et al.,* 1997; Inamdar *et al.,* 2004). The hyporheic zone may have also received an increased influx of DOC, which is a main component needed for microbial processing. The effects of increased DOC concentrations may be more apparent at the downstream end of the hyporheic flowpaths, where longer hyporheic residence time may allow for greater net effect of microbial processes on pore water geochemistry. Increased microbial processing requires oxygen or other electron acceptors, and thus may produce environments suitable for denitrification and acidification. The positive relationship between residence time and microbial processing has been shown in other studies (e.g. Zarnetske *et al.,* 2011; Briggs *et al.,* 2012). Zarnetske *et al.* (2011) showed that the greatest net decline in NO_3^- concentrations in the hyporheic zone occurred at the longest residence times within subsurface flowpaths along a stream and adjacent gravel bar.

During most of the sampling regime, DO concentrations increased in the well-connected sites, but stayed fairly constant, and much lower, in the lagged sites (Table 1.3). Concentrations in DO may increase in the upstream subsurface section due to the constant and perhaps enhanced downwelling of more turbulent, and thus DO-rich, stream water. Most likely, this steady and increased source of DO at the upstream end provides enough oxygen for respiration to occur, so that alternate electron acceptors are not utilized until farther along in the subsurface flowpath.

Sulfate concentrations start uniform between lagged and well-connected sites at baseflow (Table 1.3), most likely because the presence of SO_4^{2-}-rich gypsum weathering contributes high amounts of SO_4^{2-} to the stream system. However, during the receding limb of the storm hydrograph, the difference in SO_4^{2-} concentrations between lagged and well-connected sites becomes significant (Table 1.3). This is most likely due to SO_4^{2-} reduction, as we see lower

concentrations of SO_4^{2-} in the downstream sites. By the end of the sampling regime, as the stage recedes, SO_4^{2-} concentrations have returned to pre-event conditions (Table 1.3), again displaying the dominance of bedrock weathering across the study reach.

As there is more cumulative microbial processing at the downstream sites due to flowpath length, the dominant process of NO_3^- and SO_4^{2-} reduction is reflected in higher K^+ concentrations (Table 1.3). Concentrations of reactive K^+ are larger in the downstream sites at baseflow and the difference becomes greater throughout the storm. We hypothesize that as DOC concentrations increase, mineralization of organic matter increases as microbial processing increases. This mineralization of organic matter releases K^+ found in the organic matter (Blair, 1988) and the net effect of the longer subsurface flowpath at the downstream sites allows for higher concentrations of K^+.

There is a range in streambed storm responses within streambed groups (well-connected, lagged, and GW-rich groups), suggesting a gradation of the stream-streambed connectivity and GW influence. Our results further show that this gradation of geochemical drivers in the streambed shifts throughout the storm event. For example, we observed signs of the expansion of groundwater influence across the streambed, most notably at the head of the riffle at P03. Site P03 showed chemistry similar to SW-rich sites at pre-event baseflow conditions (PC1.1= -1.8, low concentrations of Mg^{2+}, Ca^{2+}, HCO_3^-, SO_4^{2-} and high concentrations of Na^+ and Cl^-; Figure 1.2). However, during the storm, the solute concentrations at P03 became increasingly more similar to other GW-rich sites (PC1.1>0, high concentrations of Mg^{2+}, Ca^{2+}, HCO_3^-, SO_4^{2-} and low concentrations of Na^+ and Cl^-). This shift in pore water chemistry suggests the zone of GW-influence increased during the storm event, as P03 is adjacent to or at the edge of consistently GW-rich regions (P01, P02, P05, and P09). Several modeling studies have also reported an

increase in the area of GW discharge during periods of changing stream stage (Wondzell and Swanson, 1996; Wroblicky *et al.*, 1998; Shibata *et al.*, 2004). Cardenas and Wilson (2007) and Boano *et al.* (2009) showed that the water table in the riparian zone or nearby hillslope rose during a storm, increasing the hydraulic gradient toward the stream, thus driving GW flowpaths toward the streambed and compressing the hyporheic zone. We hypothesize this rapid increase in hydraulic gradient toward the stream is causing the increase of GW influence at P03 (Figure 9).

Groundwater-rich sites do not show a large chemical response from downwelling SW (Figures 2 and 6) and thus we believe the groundwater source overwhelms the stream signal at those particular sites during the storm. We hypothesize that SW represents a sufficiently small portion of the bed chemistry at the GW-rich sites so that temporal changes in any downwelling SW chemistry do not have a large influence on the pore water chemistry. Although the increase in stream stage during the storm may reverse hydraulic gradients in some regions of the bed, or increase gradients at initially downwelling sites, we hypothesize that the rising stream stage is not sufficient to reverse the hydraulic gradient at the focused groundwater discharge zones. As a result, GW-rich sites maintain an upward gradient throughout the storm event and thus show no geochemical signs of an influx of large proportions of SW. The cause of the focused GW upwelling may be local-scale geology, such as localized areas of higher hydraulic conductivity.

4.3 Conceptual Model

The coupling of bedform morphology-driven hyporheic exchange with localized GW discharge at our study site creates complex geochemical responses to fluctuating stream stage in the streambed. In this section, we present a summary, or conceptual model, of hyporheic

exchange patterns occurring in the streambed during baseflow, storm onset, and storm recession, and the associated geochemical response within well-connected, lagged and GW-rich sites.

At baseflow, GW-rich sites are localized toward the upstream end of the streambed (Figure 1.9a), most likely due to local-scale geology, such as zones of high hydraulic conductivity. Surface water-rich sites, on the other hand, show spatial geochemical patterns driven by the riffle bedform (Figure 1.5). Hyporheic flowpaths connect the sites at the upstream end of the riffle to the sites at the downstream end of the riffle and we see expected patterns in biogeochemically reactive solutes (Kasahara and Hill, 2006; Lautz and Fanelli, 2008).

During the storm, differences in pore water geochemistry measured between upstream and downstream SW-rich sites (Figures 1.6 and 1.7; Table 1.3) are from (1) differences in source water along the hyporheic flowpaths due to a changing SW chemistry during the storm, and (2) biogeochemical processes occurring along subsurface flowpaths within the streambed, such as microbial respiration and the associated consumption of DO, NO_3^- and SO_4^{2-} reduction, production of inorganic carbon, and decline in pH.

At storm onset, stream stage rises, increasing the hydraulic head at the streambed interface, causing rapid influx of event water into the hyporheic zone. There are two possible explanations for such inundation of stream water during the rising limb. First, at streambed locations with downwelling or weak upwelling exchange rates during baseflow (Figure 1.3), we hypothesize that hydraulic gradients are increased or reversed, respectively, and these regions of the streambed are rapidly inundated with dilute event water. Alternatively, rising stage increases flow rates along shallow hyporheic flowpaths such that residences times are short and biogeochemical processes leave a minimal imprint on hyporheic water chemistry. As a result, SW-rich sites initially show similar chemical responses during storm onset; for an example, a

decrease in SO_4^{2-} concentrations and increase in NO_3^- concentrations (Figure 1.7). The influence of biochemical processes occurring along the hyporheic flowpaths is diminished at this time due to rapid inundation of stream water. This briefly produces almost uniform geochemistry across the SW-rich hyporheic zone (Table 1.3). The GW-rich sites, however, still reflect only minor influence of stream water. At these locations, we hypothesize upwelling is maintained despite the increase in stage and the GW geochemical signal remains strong (Figure 1.9b).

During storm recession, the hydraulic head at the streambed interface decreases as the stream stage decreases and the subsurface flowpaths driven by the riffle bedform once again become the main driver of hyporheic zone chemistry at the SW-rich sites. During this time, hyporheic flowpaths receive stream water that has a fluctuating geochemical composition due to a fluctuating composition of precipitation, hillslope runoff, and baseflow groundwater as the system responds to the recent storm event. Because stream water chemistry varies temporally during storm recession, stream water that downwells into the streambed at one time is not chemically the same as the stream water that downwells at a time step later. Therefore, at one point in time, the chemistry of the pore water at the upstream end of the riffle more closely reflects current SW chemistry, while the chemistry of the pore water at the downstream end of the riffle reflects the chemistry of surface water that entered the streambed at an earlier time step (Figures 1.6 and 1.7).

The subsurface flowpaths driven by the riffle bedform are the main driver of hyporheic exchange at the SW-rich sites during the storm recession and the residence time of hyporheic flowpaths produces differences in concentrations of biogeochemically reactive solutes between upstream and downstream sites (Table 1.3). By the end of the study period, toward the end of storm recession, the SW chemistry began to stabilize and non-conservative solute concentrations,

such as Cl^-, became uniform across the upstream and downstream streambed sites (Figure 1.6). However, the mean value of biogeochemically reactive solutes K^+ and DO were more different between upstream and downstream sites after the storm event, relative to before (Table 1.3). Further, NO_3^- concentrations were more significantly different (smaller p-value) between upstream and downstream sites after the storm, relative to before (Table 1.3). This suggests the disturbance from the storm event had left the downstream system at a new biological condition, perhaps from an influx of DOC. Alternatively, the site had not fully recovered by the end of sampling.

5. Conclusions

This study examined the temporal and spatial response of hyporheic zone geochemistry during a storm event. The objectives of this study were to (1) characterize spatial vertical water exchange rates and geochemical patterns in the hyporheic zone around a pool-riffle-pool bedform during baseflow, and (2) use results from principal component analyses and time-series geochemical analyses to conceptualize how different regions of the hyporheic zone respond to storm events. The primary drivers of spatial and temporal variability in streambed geochemistry around a riffle during baseflow conditions and storm events are bedform morphology and chemical composition of GW discharge and varying composition of stream water from storm inputs.

Stream water enters the streambed at the head of the riffle, due to the increase in slope across the riffle, and upwells back into the stream at the tail of the riffle. Streambed sites upstream of the riffle bedform reflected conservative solute concentrations in the stream throughout storm events, while sites downstream of the riffle showed a lagged response to

changes in solute concentrations in the stream water. We hypothesize that this is most likely due to the subsurface residence time along flowpaths connecting locations where stream water enters the streambed above the riffle to locations where that water discharges back to the stream at the tail of the riffle. Temporal variations in non-conservative solutes, however, suggest different influences of streambed processes are taking place spatially during the storm event. While upstream sites mirror non-conservative stream solute concentrations throughout the storm, downstream sites reflect the influence of oxygen consumption, acidification, sulfate reduction and denitrification in the hyporheic zone, which may be enhanced due to an increase in DOC from the storm event and from a longer residence time of pore water.

The other driver of spatial variability in the streambed is from the influence of groundwater discharge. Although the increase in stream stage may drive surface water into the streambed at the groundwater discharge points, the water table in the riparian zone or nearby hillslope likely rises in response to the storm event, increasing the hydraulic gradient toward the stream, driving GW flowpaths toward the streambed, compressing the hyporheic zone and diminishing the geochemical signature of surface water in the streambed at these locations. Since the hydraulic gradient toward the stream presumably increases throughout the storm, the zone of groundwater influence within the streambed expands, elevating Ca^{2+} and SO_4^{2-} concentrations in neighboring sites.

From this study, it is apparent that the above geochemical drivers persist throughout rapid fluctuations in the stream stage, while the relative influence of these drivers shifts at some locations over time. For instance, biogeochemical differences along subsurface hyporheic flowpaths appear and disappear on much shorter time scales than GW influence to sites neighboring GW discharge points during storms.

Few hyporheic zone studies to date have focused on temporal geochemical dynamics during storm events, most likely as a result of the relatively recent interest in hyporheic zone research and the difficulty of storm sampling. This type of study provides an opportunity for researchers to better understand the hyporheic zone response during periods where watershed-scale solute export is at a maximum. Although sampling was limited by accessibility to the mini-piezometers during Tropical Storm Irene, this study showed that spatial geochemical and nutrient processing patterns in the hyporheic zone stay persistent during periods of fluctuating stream stage, which suggests that the hyporheic zone is an important area for biogeochemical processing in the stream ecosystem across non-steady state flow conditions.

Tables

Table 1.1. Loadings and correlation coefficients of solutes for the first two principal components (PC1.1 and PC1.2) for all sites (n=111). All correlation coefficients were significant with p-values <0.10.

	PC1.1 loadings GW/SW composition		PC1.2 loadings Storm dilution function	
Solute	Loadings	Correlation Coefficient	Loadings	Correlation Coefficient
Ca^{2+}	0.40	0.95	0.20	0.25
Mg^{2+}	0.40	0.95	0.19	0.23
Na^{+}	-0.35	-0.82	0.40	0.50
K^{+}	-0.27	-0.63	0.32	0.40
SO_4^{2-}	0.41	0.96	0.15	0.18
Cl^{-}	-0.34	-0.79	0.44	0.54
F^{-}	0.33	0.79	0.27	0.34
NO_3^{-}	-0.26	-0.62	0.13	0.16
HCO_3^{-}	0.16	0.38	0.60	0.75
Eigenvalue	*5.56*		*1.55*	
% Variance explained	*61.78%*		*17.22%*	

Table 1.2. Loadings and correlation coefficients of solutes for the first two principal components for surface water rich sites (PC2.1 and PC2.2, n=77). *ns= not significant correlation coefficients with p-values >0.10.

	PC2.1 loadings Storm dilution function		PC2.1 loadings Nitrate function	
Solute	**Loadings**	**Correlation Coefficient**	**Loadings**	**Correlation Coefficient**
Ca^{2+}	0.36	0.79	-0.38	-0.49
Mg^{2+}	0.34	0.75	-0.05	*ns
Na^{+}	0.43	0.95	0.19	*ns
K^{+}	0.20	0.45	-0.39	-0.51
SO_4^{2-}	0.41	0.89	0.16	*ns
Cl^{-}	0.43	0.96	0.16	*ns
F^{-}	0.25	0.55	0.34	0.44
NO_3^{-}	0.16	0.34	0.50	0.65
HCO_3^{-}	0.30	0.66	-0.49	-0.62
Eigenvalue	*4.89*		*1.65*	
% Variance explained	*54.28%*		*18.28%*	

Table 1.3. Comparison of mean concentrations for biogeochemically reactive solutes at well-connected (P04, P06, P07, P08 and P10) versus lagged (P11, P12, P13, P14) streambed sites. Average concentrations are reported for the well-connected and lagged sites, respectively, if mean differences were significant ($p<0.10$). P-values are reported in parentheses. *ns=no significant difference in concentration between groups.

Table 3. Average concentrations and p-values from a two-tailed t-test between well-connected and lagged SW-rich sites. *ns means no significant difference in concentrations between groups.

Sampling Period:	**1**	**2**	**3**	**4**	**5**	**6**	**7**
	Baseflow	**Rising limb of storm**	**Receding limb of storm**				
SO_4^{2-}	*ns	*ns	47.27, 40.48 (0.10)	53.28, 47. 59 (0.04)	58.78, 52.67 (0.04)	61.17, 56.74 (0.07)	*ns
K^+	2.03, 2.23 (0.01)	*ns	*ns	1.56, 1.83 (0.09)	1.86, 2.5 (0.07)	1.69, 2.08 (0.01)	1.84, 2.38 (0.01)
NO_3^-	2.31, 0.95 (0.07)	*ns	1.68, 0.62 (0.02)	1.74, 0.59 (0.00)	2.20, 0.71 (0.00)	2.51, 0.84 (0.00)	1.99, 0.72 (0.02)
pH	7.87, 7.62 (0.07)	*ns	8.00, 7.81 (0.06)	7.95, 7.62 (0.03)	8.05, 7.62 (0.03)	*ns	8.00, 7.68 (0.10)
DO	5.02, 2.19 (0.03)	*ns	5.16, 2.31 (0.05)	6.81, 2.01 (0.02)	7.11, 2.13 (0.00)	6.34, 2.19 (0.01)	6.221, 2.53 (0.03)

Figures

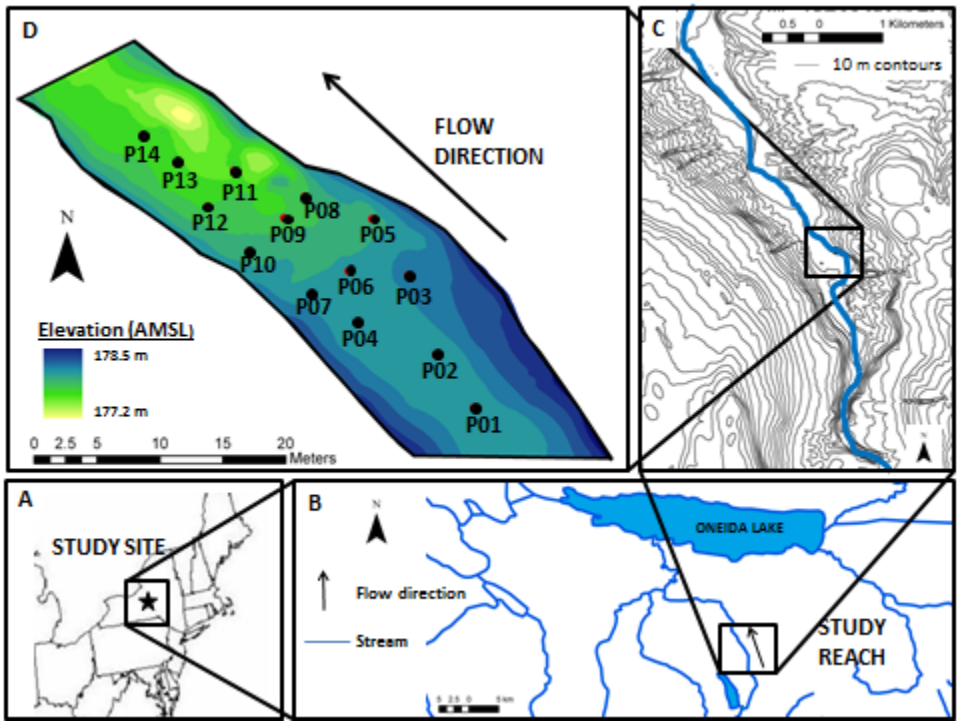

Figure 1.1. (A) Map of the study site and its location in central New York. (B) Map of Chittenango Creek watershed draining into Oneida Lake. (C) Map of elevation contours around the study reach. (D) map of study reach. Labeled black points indicate coupled installation locations for mini-piezometers and temperature profile rods. Direction of stream water flow is shown with black arrow and color shading on site map indicates streambed elevation, with blue values corresponding to higher elevations.

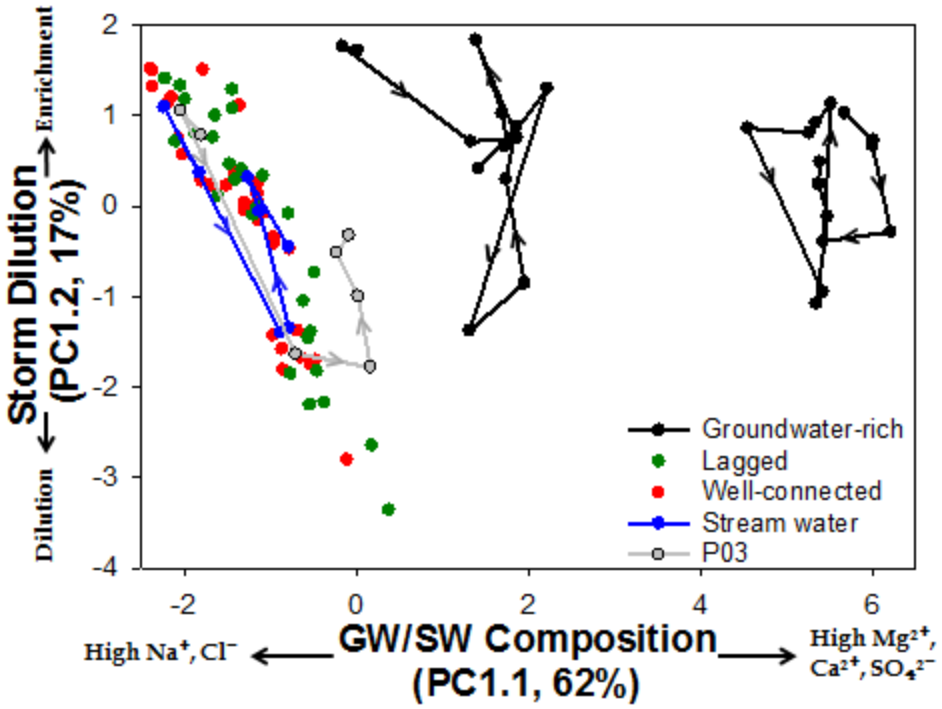

Figure 1.2. Plot of principal component 2 (PC1.2, storm dilution function) versus principal component 1 (PC1.1, GW/SW composition function) from the first principal component analysis (PC1) of all streambed sites and stream water. Blue line represents trajectory of stream water, red and green dots represents SW-rich sites (well-connected and lagged sites, respectively), black lines represent trajectory of GW-rich sites, and grey line represents trajectory of P03, the transitional site. Red and green dots follow trajectory of stream water.

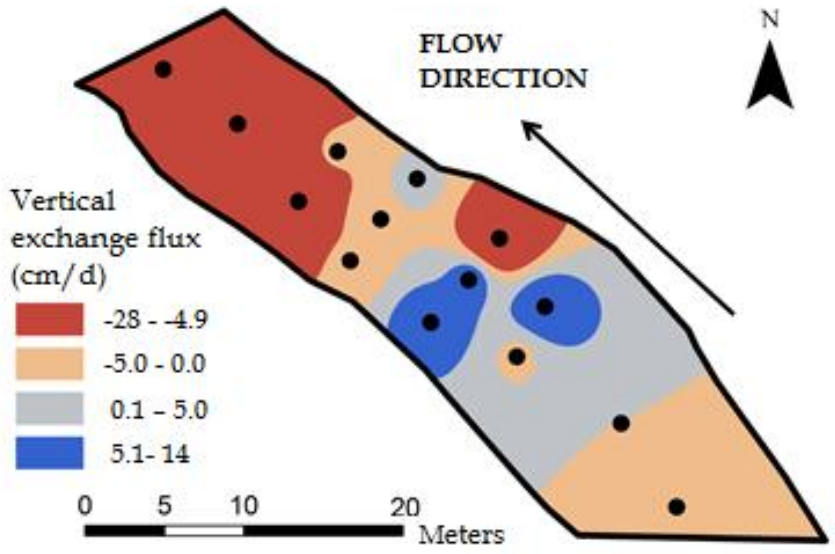

Figure 1.3. Plot of vertical exchange flux (cm/d) across the streambed averaged between 2.5 and 5.0 cm depths during baseflow conditions. Contours were interpolated using ArcGIS. Red indicates upwelling (negative values) and blue indicates downwelling (positive values).

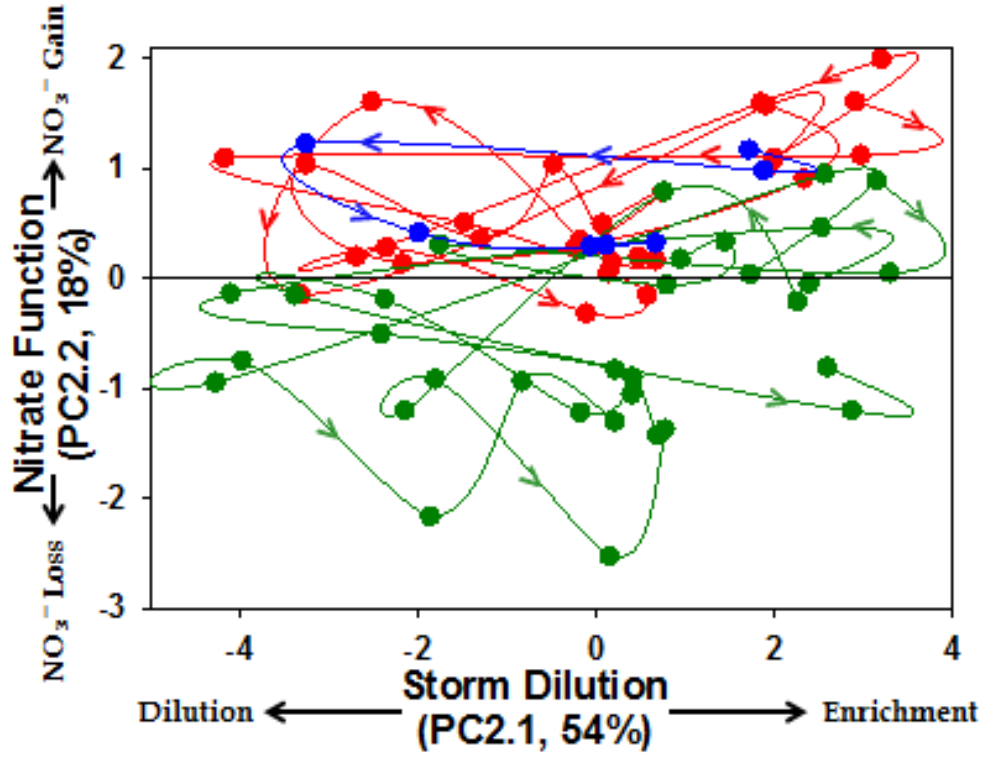

Figure 1.4. Plot of principal component 2 (PC2.2, nitrate function) versus principal component 1 (PC2.1, storm dilution function) from the second principal component analysis (PC2) of SW-rich sites and stream water. Blue line represents stream water, red line represents well-connected sites, and green represents lagged sites. All lines start in upper right corner and arrows indicate overall trajectories.

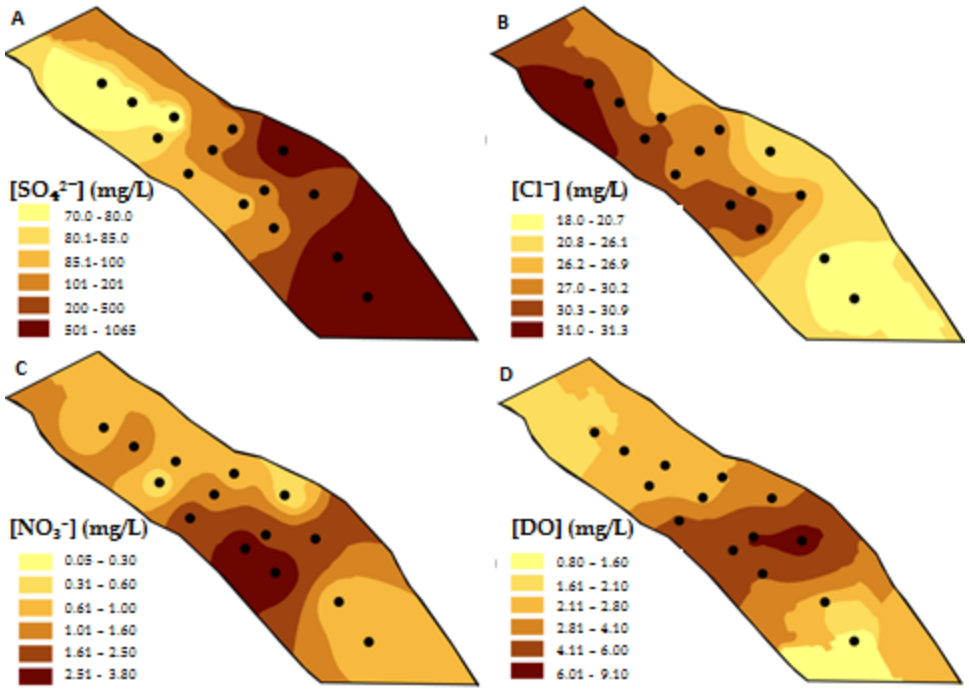

Figure 1.5. Streambed concentrations of (A) sulfate, (B) chloride, (C) nitrate, (D) and dissolved oxygen, during baseflow conditions. Lighter colors represent lower concentrations and darker colors represent higher concentrations. Contours were interpolated using ArcGIS.

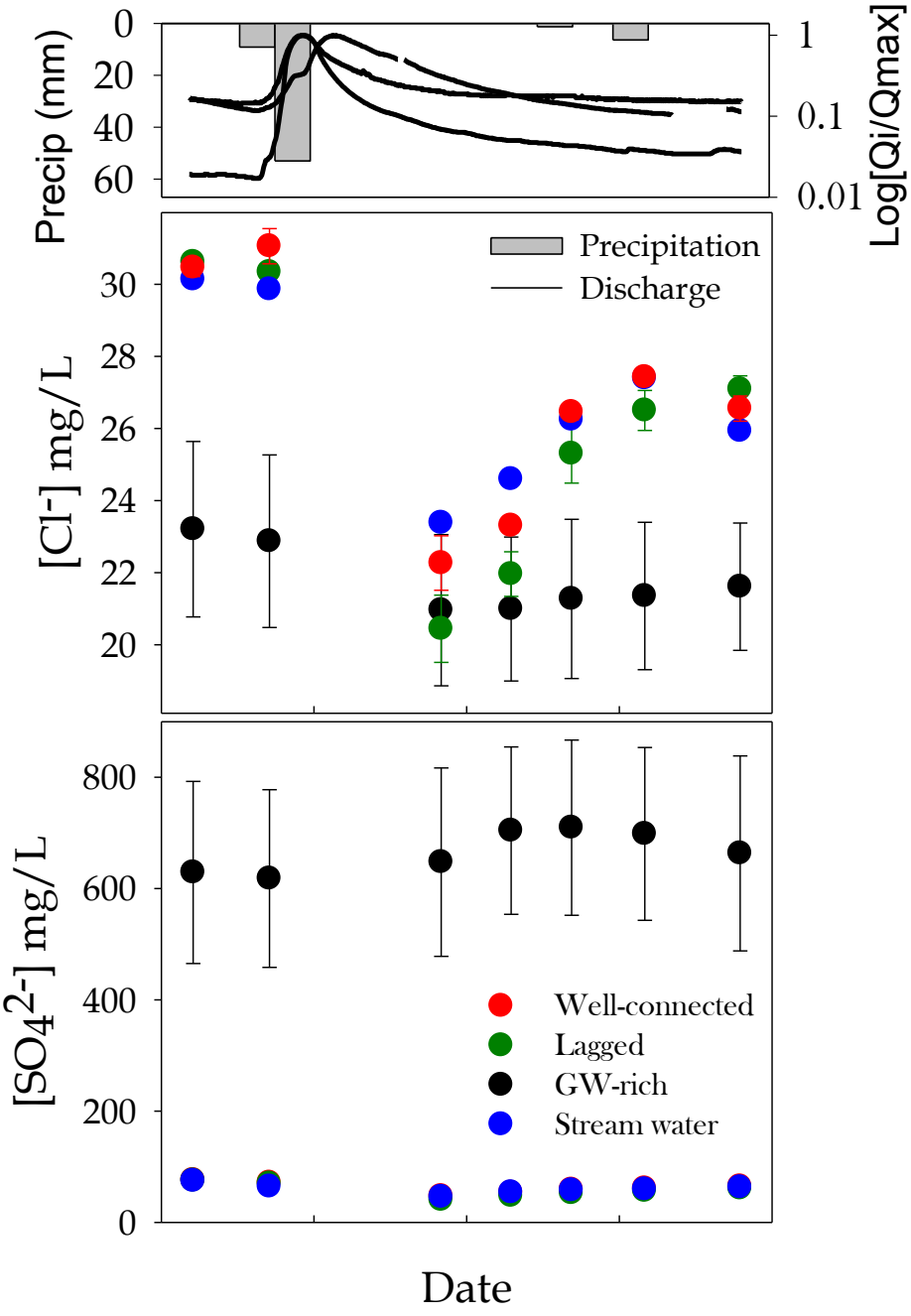

Figure 1.6. (Top) Daily precipitation inputs from nearby National Oceanic and Atmospheric Administration meteorological station. Three normalized stream hydrographs from nearby United States Geological Survey stream gauge stations. (Middle) Time series plot of mean chloride concentrations for GW-rich sites (black), lagged sites (green), well-connected sites (red), and stream water (blue). Error bars represent standard error. (Bottom) Time series plot of mean sulfate concentrations, with same color designations as middle plot.

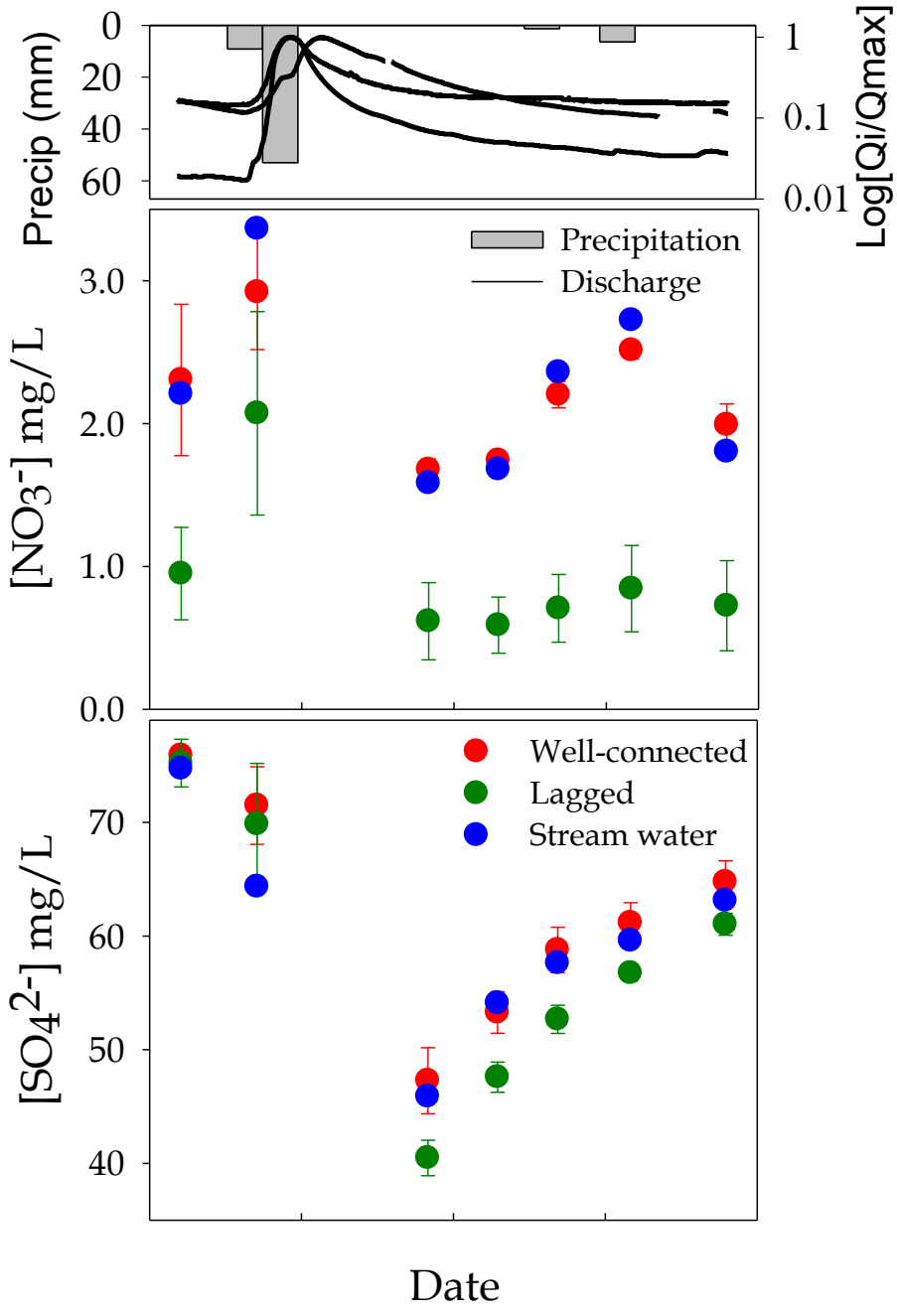

Figure 1.7. (Top) Daily precipitation inputs from nearby National Oceanic and Atmospheric Administration meteorological station. Three normalized stream hydrographs from nearby United States Geological Survey stream gauge stations. (Middle) Time series plot of mean nitrate concentrations for lagged sites (green), well-connected sites (red), and stream water (blue). Error bars represent standard error. (Bottom) Time series plot of mean sulfate concentrations, with same color designations as middle plot.

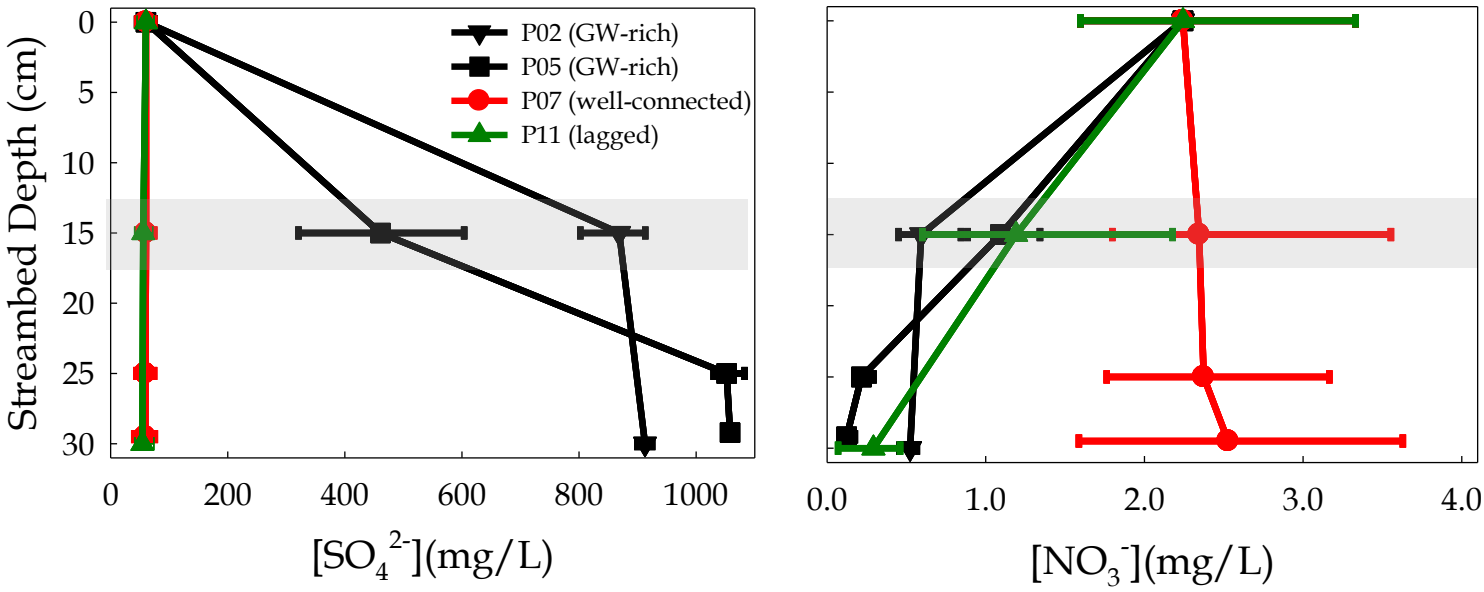

Figure 1.8. Plots of mean sulfate (left) and nitrate (right) concentrations for select GW-rich (black), well-connected (red), and lagged (green) sites at streambed depths centered at 15 cm, 25 cm, and 30 cm (5 cm screened piezometers). Error bars represent minimum and maximum values for each category. Grey box centered around 15 cm depth represents standard depth of pore water sampling. Depth of zero represents stream water.

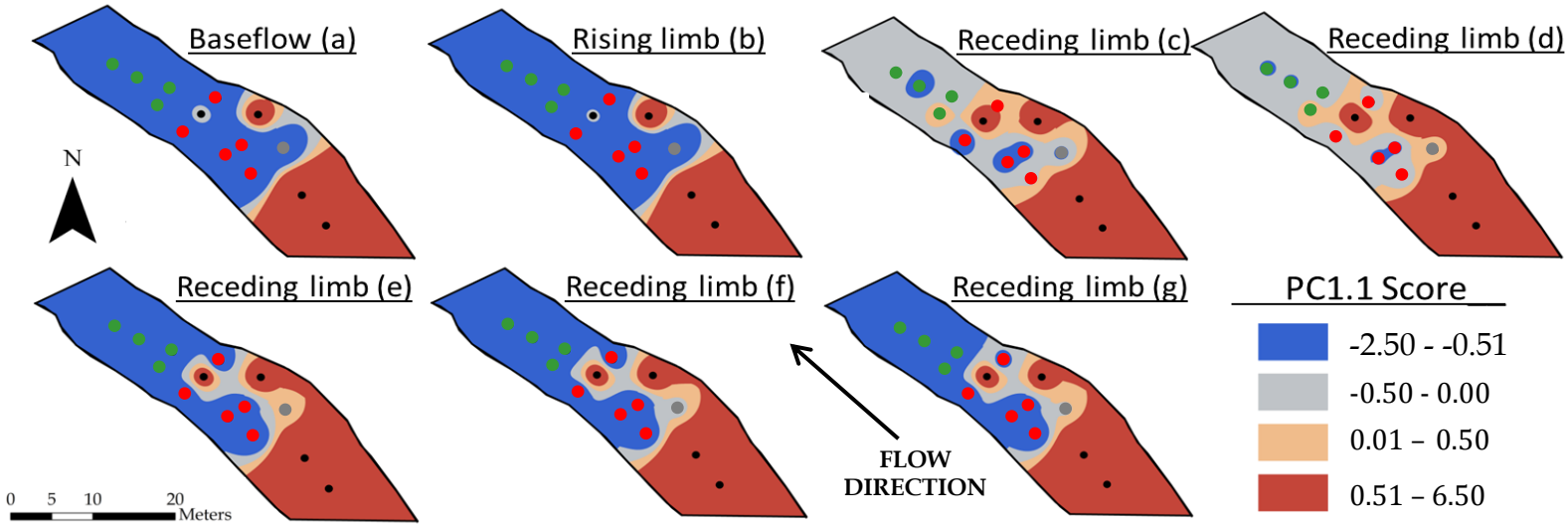

Figure 1.9. Streambed maps of the first principal component score (PC1.1 GW/SW composition score) for the first principal component analysis (PC1) over each sample date (a-g). Each piezometer site is labeled as either GW-rich (black), lagged (green), or well-connected (red). Blue contours represent more surface water influence and red contours represent more groundwater influence. Contours were interpolated using ArcGIS.

Appendix

Description: Temporal and spatial patterns of potassium concentrations as shown by a time series plot and baseflow plan view map.

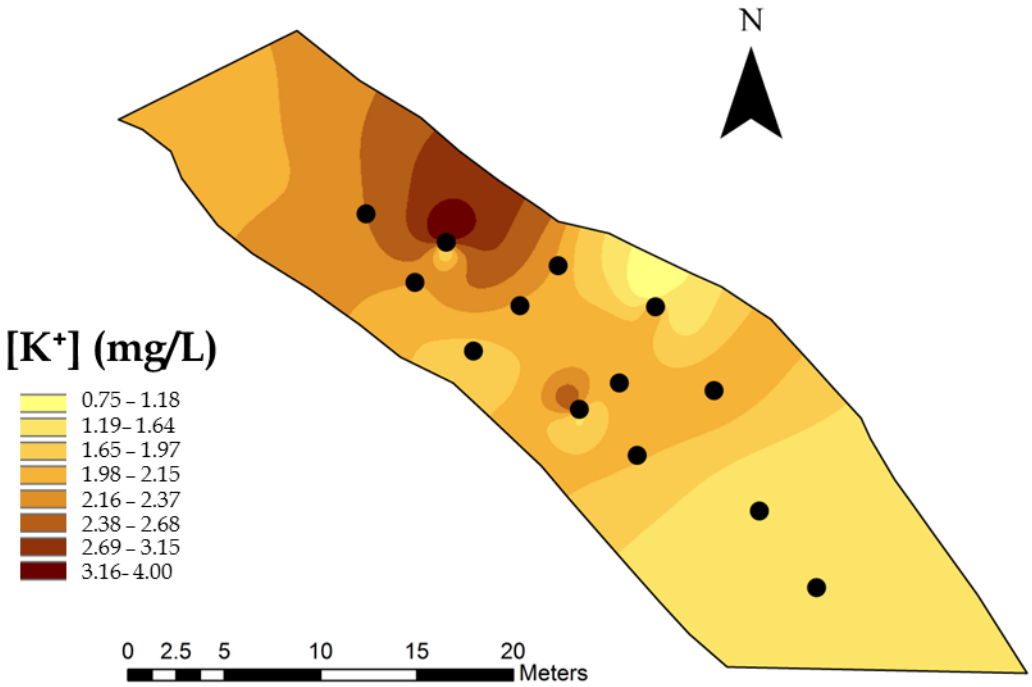

Figure A. Streambed concentrations of potassium during baseflow conditions. Lighter colors represent lower concentrations and darker colors represent higher concentrations. Contours were interpolated using ArcGIS.

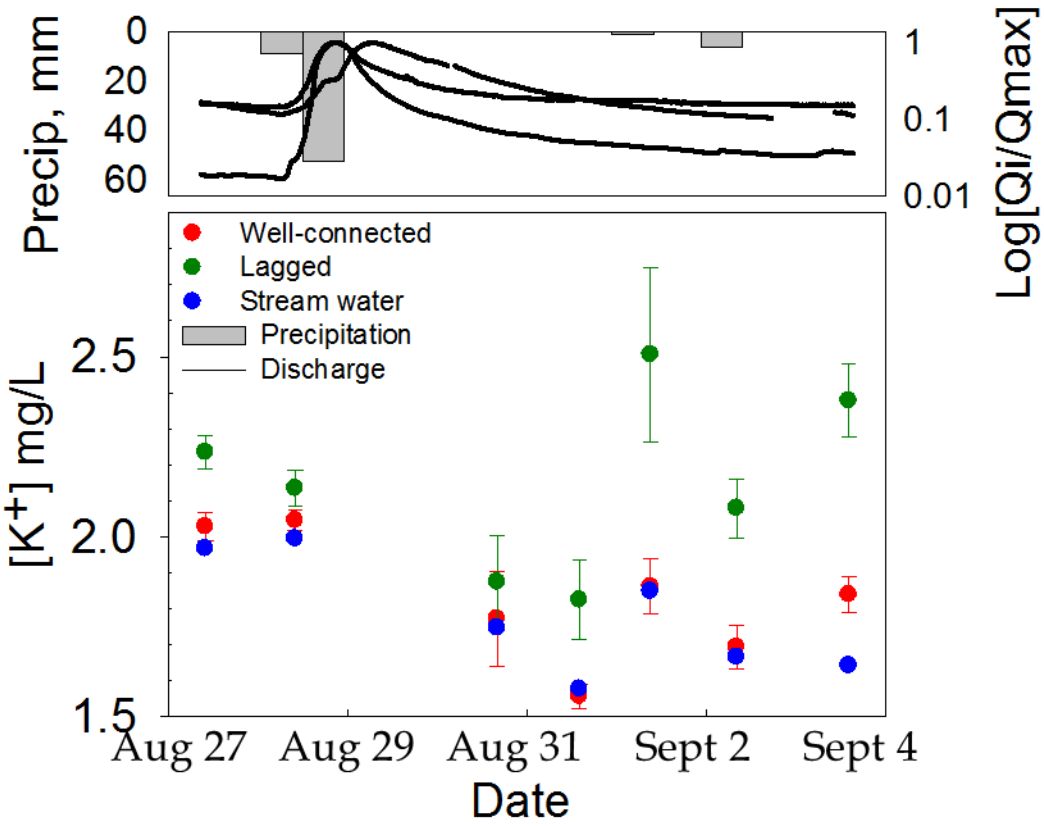

Figure B. (Top) Daily precipitation inputs from nearby National Oceanic and Atmospheric Administration meteorological station. Three normalized stream hydrographs from nearby United States Geological Survey stream gauge stations. (Bottom) Time series plot of mean potassium concentrations for lagged sites (green), well-connected sites (red), and stream water (blue). Error bars represent standard error.

Chapter 2. Pre- and post- restoration assessment of stream-ground water interactions: impacts on hydrological and chemical heterogeneity in the hyporheic zone

(Note: This manuscript is written in the style of the journal Freshwater Science)

1. Introduction:

The movement of both stream water and groundwater into and out of the streambed, commonly described as hyporheic exchange, produces unique environments for macro- and micro-invertebrates (Vervier et al 1992, Boulton et al 1998, Hayashi and Rosenberry 2002). This streambed ecotone, referred to as the hyporheic zone, provides a spectrum of subsurface habitats that range in amounts of available oxygen and nutrients, water temperature, and light intensity (Gibert et al 1990). Physical parameters, such as bedform morphology, channel meandering, aquifer hydraulic conductivity, and hydraulic gradients within and adjacent to the stream drive the distribution of stream water and groundwater in the hyporheic zone (Morrice et al 1998, Boano et al 2006, Kasahara and Hill 2006, Hester and Doyle 2007, Lautz and Fanelli 2008). This variability in water source influences the distribution of invertebrates that dwell within the hyporheic zone (Marmonier et al 1993, Brunke and Gonser 1997, Hayashi and Rosenberry 2002, Boulton 2007). These streambed invertebrates have demonstrated unique functions and contributions to stream systems, such as the alteration of streambed porosity (Edler and Dodds 1992), rates of stream and streambed metabolism (Hendricks 1996, Hakenkamp et al 2002), organic matter and pollutant breakdown (Smith and Lake 1993, Haack and Bekins 2000) and the movement of material within and through the hyporheic zone (Stanford and Ward 1993, Strayer 1994). Thus, the natural heterogeneity of stream-streambed connectivity within the subsurface is important for maintaining ecosystem function through the creation of variable habitats for invertebrates (Gibert et al 1994, Hancock et al 2005).

That said, the health of the hyporheic zone is increasingly being threatened by anthropogenic forcings, through pollution, alteration of exchange processes, and the reduction of stream-groundwater interactions from such processes as colmation (Brunke and Gosner 1997). While heterogeneity in streambed topography and streambed roughness increases hyporheic exchange (Harvey and Bencala 1993), degradation of streambed reaches from excessive sedimentation or erosion can cause homogeneous streambed topography and limit exchange rates. This in turn endangers the ability of the hyporheic zone to foster a unique environment for countless species of subsurface fauna. Without a strong stream connection, the diminished availability of dissolved oxygen, light, and nutrients will limit the productivity of the streambed and reduce the heterogeneity of invertebrates, which are important indicators of overall stream ecosystem health. This disconnection will limit the hyporheic zone only to the species that have a strong affinity to more groundwater-like habitats. In response, there has been a recent push within the research community for stream restoration that works to increase the vertical connectivity between streams and groundwater (e.g. Boulton 2007, Kasahara et al 2009, Hester and Gooseff 2010, 2011).

The U.S. spends billions of dollars each year on stream restoration (Bernhardt et al 2005), a common method used to improve ecological, physical, and chemical conditions in degraded stream systems (Lave 2009). The majority of restoration projects are small scale (< 1 km stream length) and used to improve aquatic habitat, reduce sediment erosion through bank stabilization, and improve surface water quality (Bernhardt et al 2005). Many of these small-scale projects include channel re-meandering, cross-vane installation, and bank armoring. Natural Channel Design (NCD), also known as the Rosgen method (Rosgen 1994) or river classification approach (Hey 2006), is a common tool used in river restoration, includes many of the above restoration

strategies, and is highlighted in this study. However, impact assessments occur in <10% of completed projects (Bernhardt et al 2005) and hyporheic exchange is rarely included as a goal for current restoration projects (Hester and Gooseff 2011). As a result, little is known about the effectiveness of NCD restoration on stream structure, function and hyporheic exchange.

Of the restoration structures frequently used in NCD, this study focuses on the impacts of cross-vane and engineered rock riffle installation. Cross-vanes are large boulder dams typically installed at the heads of riffles or in glides to reduce bank erosion, establish grade control, improve ecological habitat, and focus stream energy to the thalweg (Rosgen 2001). By creating a head differential from upstream to downstream of the cross-vane and focusing flow to the channel center, cross-vanes typically deepen an excavated plunge pool immediately downstream of the structure (Daniluk et al in press). When cross-vanes are paired with engineered rock riffles, however, the plunge pool is filled with boulders and cobbles, increasing turbulence and simulating a high gradient riffle (Hester and Gooseff 2011).

Restoration features that enhance hyporheic exchange do so by enhancing the physical flow of water through the streambed (Hester and Gooseff 2011). A primary driver of hyporheic exchange is the local variation in head gradients between the stream and groundwater, from such bedform topography as pool-riffle and step-pool sequences (Harvey and Bencala 1993, Kasahara and Hill 2006). Previous studies on streambed geochemistry and vertical hyporheic exchange rates around restoration cross-vanes show the hydraulic step across the structures produces high rates of downwelling immediately upstream of these structures (Lautz and Fanelli 2008, Crispell and Endreny 2009, Daniluk et al in press, Gordon et al in press), creating hotspots of hyporheic exchange. Further, heterogeneity in sediment texture and turbulence, as seen across the rock-

riffle, has also been shown to drive hyporheic flow (Elliot and Brooks 1997, Cardenas and Wilson 2007).

The majority of research examining the impacts of restoration on the hyporheic zone has focused on identifying generalizable and predictable spatial patterns in hyporheic exchange and/or streambed geochemistry around restoration structures (Kasahara and Hill 2006, Lautz and Fanelli 2008, Crispell and Endreny 2009, Gordon et al in press). Some studies have compared hydrology and geochemistry of the hyporheic zone between restored streams and reference stream reaches representing the pre-disturbance condition (Daniluk et al in press) or unrestored reaches representing the pre-restoration, degraded condition (Knust and Warwick 2009). Restoration using NCD often includes basing the restoration project design on the characteristics of natural features found at stable reference reaches (Rosgen 1998, Rosgen 2011). Reference reaches are intended to represent pre-disturbance conditions for the specific stream degradation that the restoration is aiming to address (Rosgen 2011). To date, the authors of this paper are unaware of any studies examining changes in hyporheic zone dynamics pre- and post- restoration at a single site. This paper addresses this gap in knowledge by measuring hyporheic zone exchange rates and geochemistry across the same stream reach pre- and one year post- stream restoration. The objectives of this study are to:

1. Quantify baseflow hyporheic zone exchange rates and geochemistry across a pool-riffle-pool bedform in a stream reach immediately prior to and one year after installation of a cross-vane and engineered rock riffle.

2. Examine the similarities and differences in pre- and post- restoration hyporheic exchange rates and geochemistry and provide the ecological implications of these results.

2. Methods

2.1 Site Description

The study site was a 30 m pool-riffle-pool sequence of Chittenango Creek (Figure 2.1), an ungauged tributary to Oneida Lake, near Syracuse, New York, USA (43°00' 32.27" N 75°50' 49.85" W, elevation 168 m), with a drainage area of 750 km^2. The site was restored in September 2011 with installation of a cross-vane across the head of the riffle and an engineered rock riffle immediately downstream. The cross-vane is made up of a series of large boulders and the engineered rock riffle is comprised of large cobbles. The remaining portion of the streambed is comprised of cobbles and gravel with minimal fines, the same material that was present prior to restoration. Below the surficial streambed layer, the interstitial space between the gravel is comprised of sand and silt. Measurements of streamflow with an acoustic doppler velocimeter show discharge was 0.80 m^3s^{-1} at the study reach during August 2011, at the time of the pre-restoration assessment, and 0.51 m^3s^{-1} at the study reach during August 2012, at the time of the post-restoration assessment.

2.2 Stream Instrumentation and Sampling

We surveyed the morphology of the study site pre- and post- restoration with a Nikon Nivo 5.M total station, which has a spatial resolution of <1 cm. Pre-restoration, we collected spatial information at 167 survey points to characterize position of installed sampling equipment, bedform morphology, and water edge during baseflow conditions (Figure 2.1). Post-restoration,

we collected spatial information at 219 survey points to re-characterize position of installed sampling equipment and restoration structure, bedform morphology, and water edge during baseflow conditions (Figure 2.1).

To calculate vertical exchange rates in the streambed, temperature profile rods (14 during pre-restoration, 10 during post-restoration) were installed throughout the study reach (Figure 2.1). Temperature profile rods contained seven vertically-stacked temperature sensors (iButton DS1922L, Maxim Integrated, San Jose, CA), with six installed in the streambed at 5 cm intervals to a depth of 30 cm and one positioned in the water column (depth = 0 cm). Pre-restoration, temperature sensors recorded temperature at 10-minute intervals for seven continuous days during baseflow. Post-restoration, temperature was measured at 30-minute intervals for seven continuous days during baseflow. Vertical water exchange rates at each location were calculated using one-dimensional heat transport modeling (Hatch et al 2006, Gordon et al 2012). VFLUX (Gordon et al 2012), a MATLAB computer program, was used to derive vertical exchange rates every two hours during the observation period as calculated from the difference in amplitude of the propagated diurnal temperature signal measured at multiple depths (Hatch et al 2006). Flux rates were calculated every 2.5 cm from a depth of 2.5 cm to 27.5 cm. To create profiles of how vertical exchange rates change with depth, the two-hour exchange rates were averaged over the baseflow observation period to derive a single exchange rate for each vertical observation point. For spatial comparison of vertical exchange rates in plan view between pre- and post- restoration conditions, shallow exchange rates at depths of 2.5 cm and 7.5 cm were averaged to derive one exchange rate at the streambed interface.

Pre-restoration, mini-piezometers were installed at the same 14 locations as temperature profile rods (Figure 2.1). Post-restoration, mini-piezometers were installed in 19 locations

distributed around the 10 temperature profile rods (Figure 2.1). Mini-piezometers were constructed of PVC pipe (1.27 cm ID) with a 5 cm screen created by drilling a series of 0.3 cm diameter holes in the pipe. These mini-piezometers were installed 17.5 cm below the stream-streambed interface, such that the 5 cm screen was centered at 15 cm. Plastic tubing and a syringe were used to purge and sample pore water from the piezometers. Each piezometer was purged once prior to sample extraction.

All samples were extracted within a two-hour period and filtered through a 0.7 µM glass microfiber filter within eight hours after sampling. Dissolved oxygen (DO), specific conductance (SC) and pH were measured in the field. Dissolved anions, specifically fluoride (F^-), chloride (Cl^-), nitrate (NO_3^-) and sulfate (SO_4^{2-}), as well as dissolved cations, specifically calcium (Ca^{2+}), sodium (Na^+), magnesium (Mg^{2+}), and potassium (K^+), were analyzed on a Dionex ICS-2000 Ion Chromatograph. Ammonium (NH_4^+), bromide (Br^-), and phosphate (PO_4^{3-}) were measured, but were not used in the analysis as the majority of samples registered below the instrument detection limit. Concentrations of HCO_3^- were calculated from the difference between total concentrations of anions and cations.

Rhodamine WT (RWT) is a fluorescent dye often used as a hydrologic tracer (Kilpatrick and Cobb 1985). While monitoring post-restoration conditions, we used a 24-hr constant-rate injection of RWT to calculate the percentage of surface water in streambed pore water at the 15 cm depth of each mini-piezometer at baseflow conditions. For the 24-hr period, we continuously injected RWT into the stream roughly 350 meters upstream of the study site. The plateau concentration of RWT was 11.2 parts per billion (ppb) in the stream water, as measured in the vicinity of mini-piezometer PS (Figure 2.1). After plateau was reached, we sampled stream water near PS as well as streambed pore water at each mini-piezometer every 30 minutes for the first

two hours and then every two hours for the remainder of the experiment (for a total of ten sampling periods). During the last sampling period, we also collected stream water near each mini-piezometer location. This snapshot of RWT in stream water at each piezometer location showed somewhat variable mixing of RWT across the stream reach during plateau. We assumed the variable mixing of RWT across the stream reach was constant through time and, as a result, the range of observed RWT concentrations in the stream during the last sampling period (-0.76/+1.47 ppb from measurement value at PS) was representative of the range of RWT concentrations during other times of the plateau. The assumed range of RWT concentrations in the water column across the study reach was used to estimate error of the percent surface water at each mini-piezometer.

We decanted the water samples in the field to minimize suspended sediment. We measured RWT in each sample at room temperature using an in-lab GGUN-FL fluorometer. For quality control, we measured RWT concentrations in each sample twice, corrected for temperature during measurement, and took the sample average. To calculate percent stream water in the pore water at each streambed site, we calculated the percent difference between RWT concentrations in the streambed pore water and in the stream at each time step. We then averaged the percent surface water from the 7^{th}, 8^{th}, and 9^{th} sampling period to get a single percent surface water value for each mini-piezometer location.

3. Results

3.1 Streambed Morphology: Pre- and Post- Restoration

Longitudinal streambed elevations across the pre- and post- restoration sites show markedly different morphology (Figure 2.2). Although the longitudinal change in streambed elevation is

the same pre- and post- restoration (0.2 m), the change in elevation across the reach is concentrated in the vicinity of riffle pre-restoration and the cross-vane and engineered rock riffle post-restoration (Figure 2.2). Although an engineered rock riffle was installed where plunge pools are typically excavated (Rosgen 2011), a pool was present downstream of the rock riffle, producing streambed elevations as low as those observed pre-restoration (Figure 2.2). The streambed had a 5% slope between the crest of the riffle and the bottom of the downstream pool pre-restoration. Across the restoration structure, from the highest elevation at the cross-vane to the lowest elevation in the downstream pool, the streambed had a 12% slope. Streamflow across the cross-vane and engineered rock riffle was visibly more turbulent than across the pre-restoration riffle, due to the focused flow toward the stream channel center induced by the cross-vane and the increased slope across the engineered rock riffle.

3.2 Baseflow Geochemistry and Vertical Exchange Rates

3.2.1 Pre-Restoration

During baseflow conditions, SW chemistry was dominated by SO_4^{2-} and Ca^{2+} due to gypsum dissolution from the local bedrock (Figure 2.3). Surface water showed high concentrations of DO, NO_3^-, Na^+, and Cl^- relative to streambed pore water (Table 2.1). Stream water was uniform across the stream reach, confirmed by water samples taken at the head and tail of the study reach.

Similar to the stream, pore water geochemistry was dominated by gypsum dissolution (Table 2.1, Figure 2.3). Based on the distribution of streambed solute chemistry, streambed sites can be divided into two categories: surface water (SW)-rich and groundwater (GW)-rich sites (Figure 3, Zimmer and Lautz 2013). Groundwater-rich sites have SO_4^{2-} concentrations of >200

mg/L and Ca^{2+} concentrations of >120 mg/L. Pre-restoration, the GW-rich sites were spatially oriented toward the head of the riffle and on the outside of the meander (sites P01, P02, P05, and P09; Figure 2.1) and had relatively high SC values and concentrations of SO_4^{2-}, Ca^{2+}, and Mg^{2+} (Figure 2.4a for SO_4^{2-}) and relatively low concentrations of Na^+, Cl^-, DO and NO_3^-, relative to other streambed sites (Figures 2.4c for NO_3^- and Figure 2.5). Concentrations of DO ranged from 0.8 to 4.6 mg/L in the GW-rich sites and ranged from 1.6 to 9.1 mg/L in the rest of the streambed sites (Figure 2.5). These GW-rich sites showed upwelling water in the streambed (Figure 2.6) with an average vertical exchange rate of -11 cm/d at the streambed interface.

Surface water-rich sites had relatively low concentrations of SO_4^{2-}, Ca^{2+}, and Mg^{2+} and high concentrations of Na^+, Cl^- and NO_3^- relative to GW-rich streambed sites (Figures 2.4a, c). Streambed pore water geochemistry outside of zones affected by GW discharge showed spatial organization of some solutes around the riffle. Mean concentrations of most major cations (Mg^{2+}, Ca^{2+}, Na^+), major anions (HCO_3^-, Cl^-, F^-, SO_4^{2-}) and SC showed no significant difference ($p>0.10$) between piezometers upstream and downstream of the riffle. That said, mean concentrations of biogeochemically reactive ions (NO_3^- and K^+) as well as pH and DO were significantly different ($p<0.10$) at piezometers above the riffle relative to below the riffle. There was higher NO_3^- at the upstream sites and higher K^+ at the downstream sites (Figure 2.4c for NO_3^-). Heat tracing results indicated water downwelling into the streambed within the riffle with average vertical exchange rates of 9.0 cm/d across the streambed interface (Figure 2.6). Sites above the riffle showed relatively neutral exchange rates at the bed interface while sites below the riffle showed upwelling (Figure 2.6). Although some sites showed slight upwelling at shallow depths, vertical exchange rates are neutral or slightly downwelling for all sites below 10 cm (Figure 2.7).

3.2.2 Post-Restoration

During baseflow conditions, stream and pore water concentrations of solutes were relatively similar pre- and post- restoration, although solute concentrations were slightly higher (except K^+, NO_3^-, and DO) in post- restoration conditions (Table 2.1, Figure 2.3). Post-restoration, SW was still dominated by SO_4^{2-} and Ca^{2+}, with higher values of Na^+, NO_3^-, Cl^-, HCO_3^-, and DO relative to pore water (Table 2.1). Stream water was still uniform across the stream reach, confirmed again by water samples taken at the head and tail of the study reach.

Streambed pore water geochemistry was still dominated by gypsum dissolution and the ranges of solute concentrations observed in the hyporheic zone post-restoration were similar to those observed pre-restoration (Table 2.1, Figure 2.3). Similar distinctions between SW-rich and GW-rich sites were identified pre- and post- restoration. For instance, zones of GW discharge, as designated by geochemistry, were still prominent in the upper portion of the study reach, but had increased in spatial extent downstream of the structure (sites PC, PD, PE, PN, PO, and PP, Figure 2.4b). The zones of GW discharge still had relatively high concentrations of SO_4^{2-}, Ca^{2+}, and Mg^{2+} and low concentrations of Na^+ and Cl^-, relative to other streambed sites (Figure 2.4c for SO_4^{2-}). These GW-rich sites had high SC values ranging from 855 to 1979 μS/cm, whereas the rest of the streambed sites had stream-like SC values from 652 to 746 μS/cm. Concentrations of DO ranged from 0.6 to 1.1 mg/L in the GW-rich sites and ranged from 0.6 to 8.5 mg/L in the rest of the streambed sites (Figure 2.5). These GW-rich sites showed upwelling water in the streambed (Figure 2.6) with average vertical exchange rate of -3.3 cm/d across the bed interface. Although geochemistry suggests GW-influence had expanded downstream of the structure

(Figure 2.4b), heat tracing results are less conclusive, as temperature profile rods do not cover the same spatial extent as mini-piezometers (Figure 2.1).

Surface water-rich sites had relatively low concentrations of SO_4^{2-}, Ca^{2+}, and Mg^{2+} and high concentrations of Na^+, Cl^- and NO_3^- relative to GW-rich streambed sites (Figure 4b, d). Streambed pore water geochemistry showed spatial organization around the structure and rock riffle. For instance, K^+ had high concentrations while DO had low concentrations immediately downstream of the restoration structure. Concentrations in NO_3^- were low upstream of the structure and in GW discharge zones, but were high adjacent to the structure, in the rock riffle, and in the upstream section of the next riffle.

The magnitude of downwelling increased substantially after restoration; the highest exchange rate at the streambed interface pre-restoration was 15 cm/d, while the highest average exchange rate post-restoration was 290 cm/d (Figure 2.6). At the streambed interface, downwelling was highest immediately upstream of the restoration structure, with ranges between 170 to 290 cm/d (Figure 2.6). Within the rock riffle, there was strong downwelling at the shallow depths (1.0 to 86 cm/d), but exchange rates decreased with depth and became neutral or slightly downwelling, except for one site in the rock riffle that showed slight upwelling (Figure 2.7).

3.3 Percent Stream Water in Streambed: Post-Restoration

A 24-hour constant rate injection using RWT was used to calculate the percentage of stream water in the streambed. The average concentration of RWT in the stream over six hours during the plateau period of the experiment was compared to the average concentration of RWT in the pore water at each mini-piezometer location during that same time. The concentration

range of RWT in the stream water from uneven mixing across the stream reach provided errors in percent stream water in the streambed between 7-12 percent. Streambed sites PG, PH, PI, PJ, PK and PL showed stream water presence around 100 percent, while the majority of the other streambed sites showed roughly 20 percent stream water (Figure 2.8). The sites with high stream water mixing were located around the restoration structure (Figure 2.8). Site PM was within the engineered rock riffle, but showed lower percent surface water (~30%), as well as lower concentrations of DO, relative to other sites within the engineered rock riffle. PQ was located at the tail of the engineered rock riffle, but showed high percentage of stream water (~60%) as well as high concentrations of Cl^- and DO, relative to adjacent sites. Similarly, PF, located in the pool above the restoration structure, had higher percent stream water (~35%), and showed higher concentrations of Cl^- and lower concentrations of SO_4^{2-} than nearby sites.

4. Discussion

4.1 Zones of Upwelling and Downwelling Pre- and Post- Restoration

The pre- and post- restoration exchange rates are similar to values seen at reference and restored reaches, respectively, in other studies conducted in central New York, USA (Daniluk et al in press, Gordon et al in press). While neither study compared post-restoration exchange rates to pre-restoration exchange rates at any of the sites, these studies are in geographically similar locations and use similar methods for calculating vertical exchange rates as this study. Daniluk et al (in press) and Gordon et al (in press) showed that the streambed throughout reference reaches, as well as areas distant from structures at restored reaches, showed minimal (<40 cm/d) rates of upwelling or downwelling at the bed interface. This study found similar values at the pre-restoration site as well as in areas distant from the structure post-restoration. Similar to our study,

Daniluk et al (in press) and Gordon et al (in press) showed strong downwelling into the streambed (50-350 cm/d) adjacent to the restoration structures.

Restoration produced downward exchange rates that were an order of magnitude larger than pre-restoration, specifically adjacent to the restoration structure (Figures 2.6 and 2.7), due to an increase in the water surface slope and the surface water turbulence across the cross-vane and engineered rock riffle. Exchange rates were similar pre- and post- restoration >1 m away from the structure and riffle bedform. The geochemistry confirms the heat tracing results. Pre-restoration, the zone of lower SO_4^{2-} concentrations, suggestive of less GW and thus more SW inputs, was focused around the inner edge of the meander within and downstream of the riffle (Figure 2.4a). Post-restoration, the zone of lower SO_4^{2-} concentrations had become more prominent adjacent to the structure (Figure 2.4b), suggestive of more streambed interaction with stream water.

For both pre- and post- restoration, geochemical analyses and heat tracing showed groundwater upwelling was prominent (Figures 2.4 and 2.6). However, the spatial resolution from heat tracing was too coarse to compare any change in the spatial extent of groundwater upwelling across the two scenarios. Streamed geochemistry indicates, through high concentrations of SO_4^{2-}, there was strong upwelling in the pool above both the unrestored riffle and the cross-vane. However, because only two piezometers were installed in the upstream pool in the pre-restoration assessment, it is difficult to conclude if the extent of groundwater upwelling in that region had changed (Figure 2.4a, b). On the other hand, it appears the zone of groundwater upwelling across the tail of the unrestored riffle bedform expanded in size after restoration. Piezometers in both scenarios spanned the width of the streambed in this area and showed that the geochemical signal of groundwater upwelling, as indicated by high

concentrations of SO_4^{2-}, extended only partially across the channel in the pre-restoration survey, but entirely across the channel width in the post-restoration survey (Figure 2.4a, b for SO_4^{2-}). This discrepancy may be due to changes in hydraulic conductivity in the streambed. The introduction of less consolidated streambed material from the construction of the engineered rock riffle may have provided pockets of high hydraulic conductivity and thus more groundwater upwelling. Another explanation could be that the presence of heavy machinery during restoration may have consolidated the bed material and lowered the localized hydraulic conductivity, which may have caused the upwelling groundwater to be pushed toward the edges of the stream channel, to areas less compacted, expanding the zone of groundwater influence.

Daniluk et al (in press) compared restored stream reaches to nearby reference reaches representing the pre-disturbance conditions. These authors observed more groundwater upwelling in the reference reaches, which may suggest restoration did not enhance the groundwater connection to the streambed. On the other hand, our results suggest restoration enhanced groundwater connection to the streambed. This discrepancy may be because the post-restoration assessment occurred one year after restoration, while the restoration in Daniluk et al (in press) was 6-8 years old and Daniluk et al (in press) compared restored and references reaches found on different stream reaches, whereas our study was a pre- and post- restoration assessment of the same stream reach.

4.2 Biogeochemical Differences Pre- and Post- Restoration

Although it is difficult to compare biogeochemistry across the two study dates because of differences in stream discharge and temporal variations in stream water chemistry, relative differences can be interpreted. Spatial patterns in conservative solutes, such as SO_4^{2-}, confirmed

heat tracing results with regard to the physical upwelling and downwelling of water within the streambed, as described in Section 4.1. On the other hand, spatial patterns in non-conservative solutes are key indicators of differences in biological activity and nutrient processing within the streambed pre- and post- restoration.

The range in DO concentrations was similar between the pre- and post- restoration assessments, with slightly higher DO in the stream and pore water pre-restoration (Table 2.1). Although NO_3^- concentrations were similar in the stream pre- and post- restoration, NO_3^- concentrations had a larger range in pore water pre- restoration. Nitrate concentrations at four streambed sites (29% of sites) were higher than in the stream during pre-restoration conditions (between 0.2 and 1.5 mg/L higher), yet only one streambed site (5% of sites) showed higher NO_3^- concentrations than stream water (0.3 mg/L higher) in post- restoration conditions (Figure 2.5). This suggests that either nitrate production is not occurring at as high a rate post-restoration, relative to pre-restoration, or that residence times in the streambed are too short post-restoration for the byproducts of nitrate production to accumulate in streambed pore water. Daniluk et al (in press) and Gordon et al (in press) also do not see strong evidence of nitrate production at restored sites.

The distribution of DO and NO_3^- concentrations in pore water across the streambed was markedly different pre- and post- restoration. Pre-restoration, there was a wide variability of NO_3^- and DO concentrations observed across the streambed sites (Figure 2.5). Post- restoration, however, there was a bimodal distribution for both constituents (Figure 2.5). There were high concentrations of DO and NO_3^- around the areas of the hydraulic steps (i.e. riffle and cross-vane) pre- and post- restoration. Post-restoration, sites adjacent to the cross-vane had NO_3^- concentrations almost identical to the stream, while sites within the pre-restoration riffle had

concentrations similar to the stream as well as chemically altered by nitrate production. Post-restoration, sites away from the structure showed much lower and almost identical NO_3^- concentrations, while sites away from the pre-restoration riffle showed a spectrum of NO_3^- concentrations (Figure 2.5). The observed spatial patterns of NO_3^- and DO concentrations pre- and post- restoration suggest a broad spectrum of net NO_3^- production and NO_3^- uptake across the hyporheic zone pre-restoration, but only either net NO_3^- uptake or conservative transport in the hyporheic zone post-restoration. The bimodal distribution of NO_3^- and DO concentrations post-restoration suggest a bimodal distribution of residence time in the hyporheic zone; very short residence times correspond to conservative NO_3^- transport, while longer residence times correspond to low DO and net NO_3^- uptake. Similarly, the Rhodamine WT constant rate injection conducted post-restoration demonstrated a bimodal distribution of percent stream water in the streambed; one group of streambed sites located adjacent to the restoration structure was comprised of roughly 100% stream water, while the other sites located away from the structure were comprised of roughly 20% stream water (Figure 2.8).

4.3 Ecological implications

Boulton et al (1998) argued the importance of the hyporheic zone as an ecotone between stream and ground water and thus a unique habitat for microbes and invertebrates. These streambed organisms provide valuable ecosystem services in the transformation and retention of nutrients in the streambed, increased porosity through burrowing, and the addition of carbon and other available nutrients through physical addition or mortality. In response to the increasing number of stream restoration sites, there has been a push toward promoting vertical connectivity as a goal in restoration projects (Boulton et al 2007, Kasahara et al 2009, Hester and Gooseff

2010). It has become apparent that although restoration practices typically do not target improvements in stream-groundwater connectivity, structures that produce hydraulic steps, specifically cross-vanes, engineered riffles, and log jams, increase hyporheic exchange (Kasahara and Hill 2006, Lautz and Fanelli 2008, Daniluk et al in press) and thus the opportunity for microbial activity and nutrient transformation (Brunke and Gonser 1997).

We saw an increase in the zone of GW discharge to the streambed at the tail end of the rock riffle. This suggests that the engineered rock riffle introduced new groundwater flowpaths, allowing for a larger extent of GW discharge at the site. These zones of GW discharge may act as areas of refugia during large scale disturbance, such as floods, as stream water may not infiltrate as far into the bed at these locations. Or instead, these zones may hinder microbial activity, due to low levels of DO and available nutrients from the lack of infiltrating stream water, thus decreasing the productivity of the streambed at these locations. Although this dynamic may be site specific, it is important to understand the influence of introducing heavy machinery or new rock material on streambed hydraulic conductivity and connections to groundwater.

The bimodal distribution of SW-rich and SW-poor streambed sites has implications for the utility of restoration for hyporheic zone health. While restoration in this study produced more streambed sites with pore water that resembles the stream, the net impacts of biogeochemical processes are not as evident post-restoration. Although there has been a recent push for restoration that includes increasing the in-stream hydraulic gradient (e.g. through step-pools, engineered riffles, etc.) in order to induce hyporheic exchange (Hester and Gooseff 2010, 2011), evidence from this study suggests securing hyporheic health through restoration is not as simple as maximizing downwelling. Most likely, there needs to be a balance between the inundation of

available DO and nutrients from stream water and sufficiently long enough residence times for such processes as nitrate production to create a net change in pore water concentrations. As is, the bimodal distribution of non-conservative solutes in the restored reach produces more homogeneous conditions in the streambed, when compared to pre-restoration, which leads the authors to question the functionality of downwell-inducing structures. Findlay (1995) explained that biogeochemical reactions in the hyporheic zone are controlled by the rate of processing as well as the percent of stream water cycling through the system. It is apparent in our study that in areas with higher percentages of stream water (adjacent to the restoration structure; Figure 8), the rate of processing is too slow and/or the short residence time minimizes the net change in pore water nutrient concentrations. On the other hand, the other areas of the streambed that show low percentages of stream water infiltrating also show depleted concentrations of DO and NO_3^-. This suggests in areas not immediately adjacent to the cross-vane, the rate of stream interaction with the streambed is too uniformly low to stimulate a spatially dynamic habitat. It is clear from our study that restoration limits NO_3^- production across the restored stream reach and the spatial heterogeneity of available DO and nutrients in the streambed seen prior to restoration is gone.

Fanelli and Lautz (2008) showed between 6.6-93.6 cm/d seepage fluxes upstream of a small, engineered log dam in Red Canyon Creek Wyoming, almost 200 cm/d slower than seen adjacent to the cross-vane in this study. With these smaller flux rates, Fanelli and Lautz (2008) showed a more patchy presence of redox-processing in the streambed, with streambed sites that were stream-like, oxic, or anoxic. Currently, in our restored reach, the patchiness is confined to sites that are either stream-like or anoxic (Figure 6). While the engineered rock-riffle installed immediately downstream from the cross-vane produce vertical exchange rates more similar to

rates seen by Fanelli and Lautz (2008), rock-riffles are not always paired with cross-vane installation.

Gordon et al (in press) calculated approximately 0.4% of stream discharge in a 50 m restored reach enters into the streambed. It is clear that although cross-vanes increase the rate of vertical exchange of stream water into the streambed, the total percentage of stream water that interacts with the streambed is still not large. This is most likely due to the spatially constrained impact of cross-vanes on vertical connection; sites immediately adjacent to the structure see high rates of downwelling, but sites >1m away do not see any changes in exchange rates. With such low volumes of stream flow exchanging with the hyporheic zone around restoration structures, there is low potential for hyporheic exchange to have a net impact on surface water chemistry along restored reaches. Although the percentage of stream water interacting with the hyporheic zone is low, hyporheic exchange still has potential to improve stream ecosystem health by promoting diverse streambed habitat to support micro- and macro-invertebrate communities. A key component of good benthic habitat is diversity. Unfortunately, it appears that NCD structures, such as cross-vanes, promote a more uniform hyporheic zone due to rapid downwelling, which may not improve overall stream ecosystem function. With the high cost of cross-vane installation and the inconclusive improvement of stream-groundwater interactions, the authors of this study suggest we explore alternative restoration practices that improve the vertical connection within stream systems using more modest hydraulic steps or designs that increase vertical exchange over a larger spatial extent than just immediately adjacent to structures.

5. Conclusion

This study examined the spatial response of streambed geochemistry and vertical exchange rates to in-stream restoration across a riffle bedform. Although recent studies have examined these parameters around restoration structures or compared restored reaches to reference reaches, to date there have been no studies the authors are aware of that track the impacts of restoration on streambed exchange rates and geochemistry on a single stream reach. We paired baseflow pore water geochemical analyses with calculations of vertical exchange rates from heat tracing in order to compare pre- and post- restoration conditions. When compared to pre-restoration conditions, the restored site had a steeper slope across the structure, which included a cross-vane and engineered rock riffle. This hydraulic step enhanced downward vertical exchange rates adjacent to the structure by an order of magnitude. These hot spots of vertical exchange introduced solutes and dissolved oxygen into the streambed, as shown by streambed solute concentrations more similar to stream water at the restored site. However, the greater vertical exchange rates decreased the residence time of water in the subsurface, which minimized the net effects of nutrient processing and promoted a bimodal distribution of geochemistry, percent stream water in streambed, and vertical exchange rates. When compared to pre-restoration conditions, the streambed was more homogeneous and the functionality of the restoration for promoting heterogeneity in hyporheic zone habitat remains questionable. Although there is a current push for the inclusion of vertical connectivity as a goal for restoration, the installation of cross-vanes creates uniform, high magnitude downwelling of stream water into the hyporheic zone, apparently decreasing diversity of processing, habitat and function.

Groundwater discharge in the post-restoration study had a greater zone of influence around the tail end of the rock riffle. The larger zone of groundwater upwelling is hypothesized to be from a change in streambed hydraulic conductivity. Localized hydraulic conductivity may have increased from the installation of loose cobbles and boulders across the rock riffle, which may have allowed for more groundwater discharge. Hydraulic conductivity may also have been decreased from compaction by heavy machinery during the restoration process, which may have caused groundwater to be flushed out toward new discharge locations. This increase in the zone of groundwater upwelling may provide more areas for refugia for organisms during periods of high disturbance. The above findings suggest that restoration enhanced both the streambed connection with stream water as well as with groundwater, however the ability for restoration to improve the functionality of the hyporheic zone remains questionable. Future studies should continue to monitor this stream site as the restoration structure evolves through time.

Tables

Table 2.1. Mean solute concentrations in stream water and mean with range of solute concentrations in pore water pre- and post-restoration. [a] From temperature profile rods at 0 cm depth (in stream column) averaged over two hour sampling period at all profile locations. [b] From temperature profile rods at 15 cm streambed depth averaged over two hour sampling period at all profile locations.

	Stream		Pore water	
	Pre-restoration	Post-restoration	Pre-restoration	Post-restoration
Ca^{2+}	77.5	89.4	144.2 (78.5 - 395.3)	170.0 (85.2 - 371.8)
Mg^{2+}	19.2	21.4	24.2 (18.0 - 48.5)	29.3 (18.4 - 52.1)
K^{+}	2	1.5	2.0 (1.3 - 2.4)	1.7 (1.5 - 2.1)
Na^{+}	18.1	22.4	17.2 (11.9 - 19.0)	18.5 (9.0 - 22.5)
SO_4^{-}	74.7	87.4	235.1 (71.8 - 906.1)	319.8 (77.5 - 924.8)
NO_3^{-}	2.2	2.1	1.5 (0.1 - 3.8)	1.2 (0.0 - 2.4)
Cl^{-}	30.1	33.8	28.4 (19.2 - 31.3)	28.5 (13.6 - 34.27)
F^{-}	0.1	0.2	0.2 (0.1 - 0.4)	0.2 (0.1 - 0.4)
HCO_3^{-}	234.3	270	259.8 (230.2 - 308.2)	259.8 (201.8 - 307.4)
DO	12.1	9.2	3.7 (0.8 - 9.1)	3.1 (0.5 - 8.5)
SC	541	677	853.4 (580.0 - 1945.0)	1043 (652-1979)
Temp	21.4 (20.8-21.9)[a]	20.0 (19.2-20.6)[a]	20.0 (18.0-21.6)[b]	17.9 (16.7-18.5)[b]

Figures

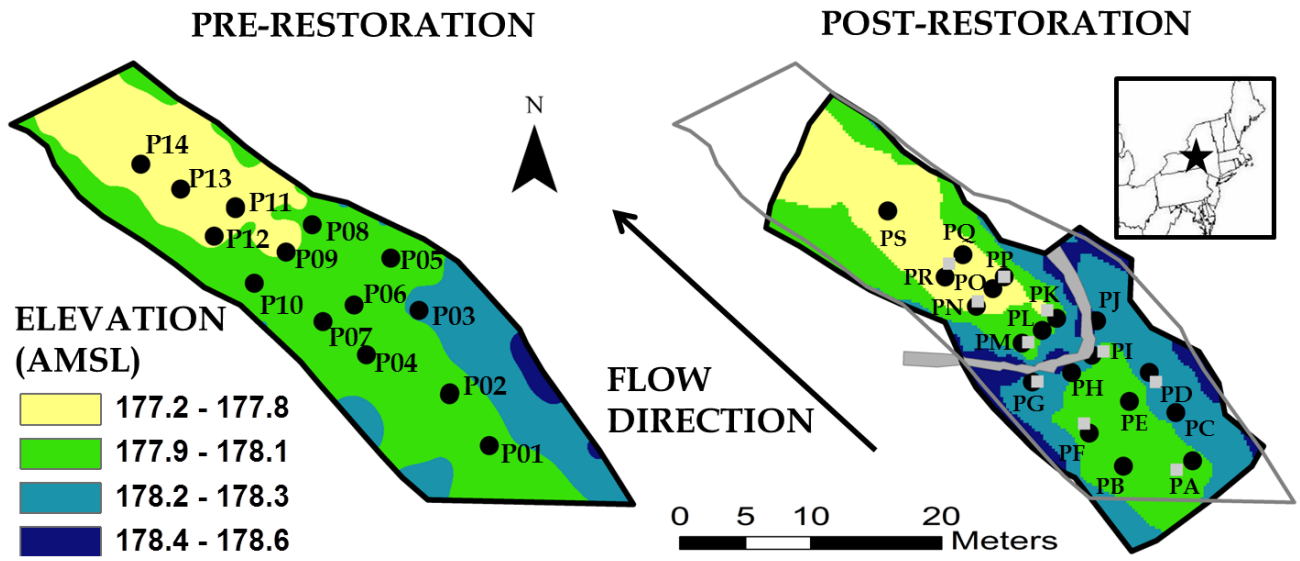

Figure 2.1 Map of study reach pre- and post- restoration. Labeled black points indicate installation locations for mini-piezometers and grey points indicate and temperature profile rods (same location as mini-piezometers pre-restoration). Direction of stream water flow is shown with black arrow and color shading on site map indicates streambed elevation, with blue values corresponding to higher elevations.

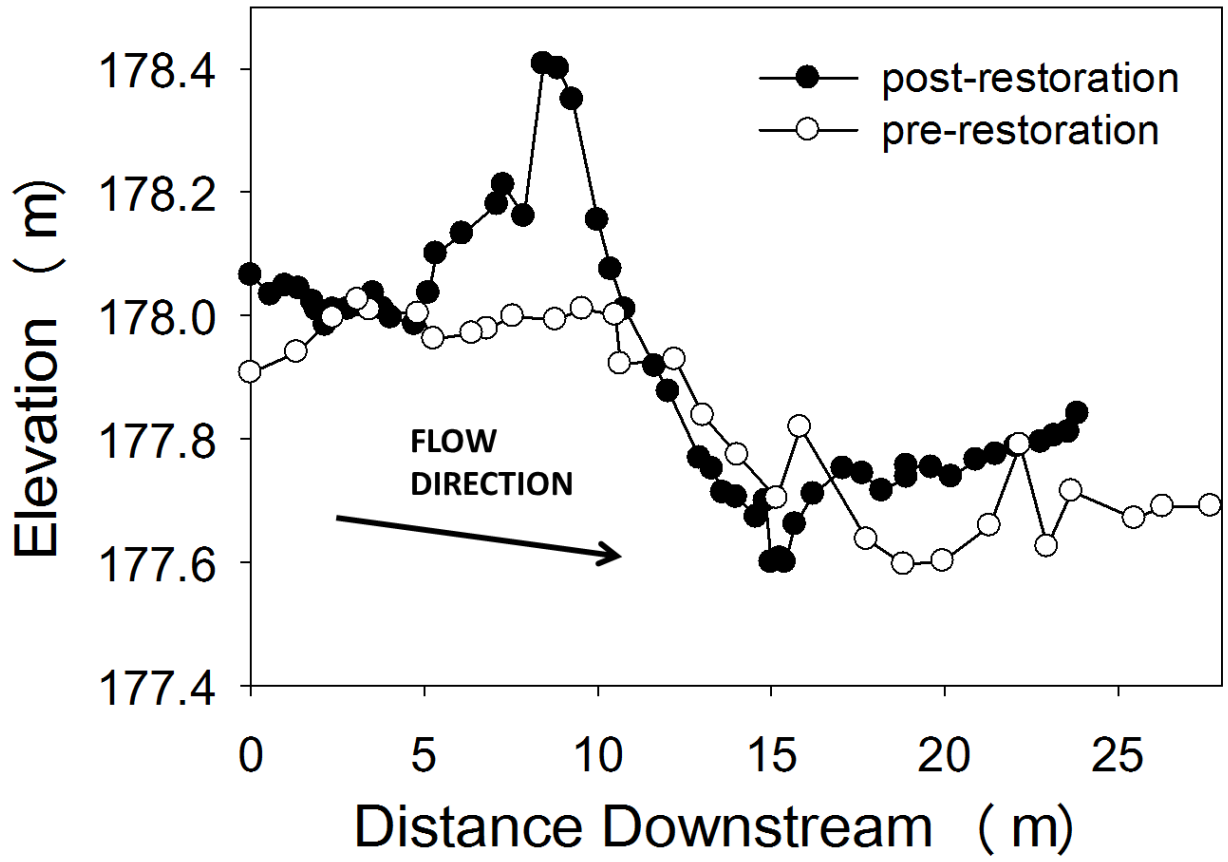

Figure 2.2 Cross-section of streambed topography. Open dots represent pre-restoration and black dots represent post-restoration.

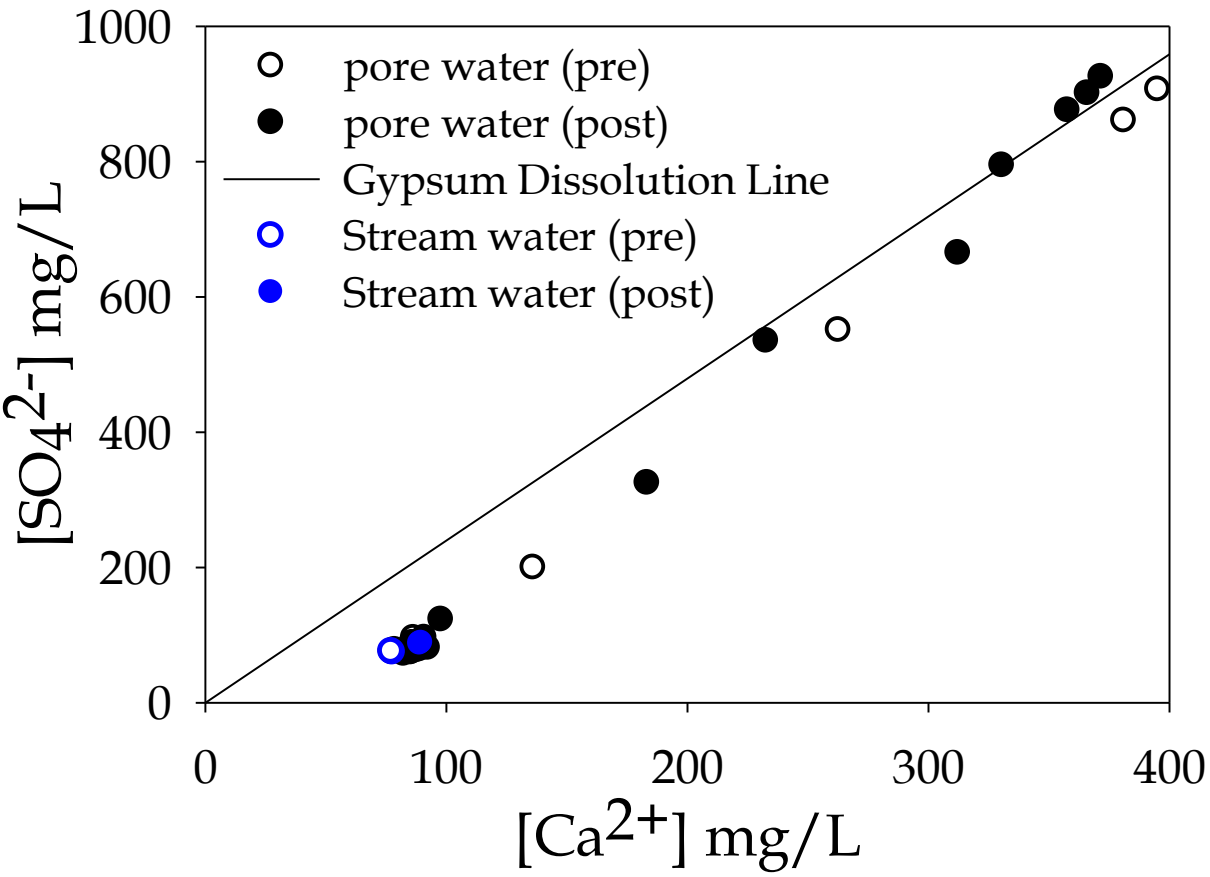

Figure 2.3. Stream water and pore water samples from pre- and post- restoration for sulfate versus calcium concentrations. Gypsum dissolute line is represented with black line. Sites that have calcium and sulfate concentrations above 100 mg/L and 200 mg/L, respectively, are considered groundwater-rich sites.

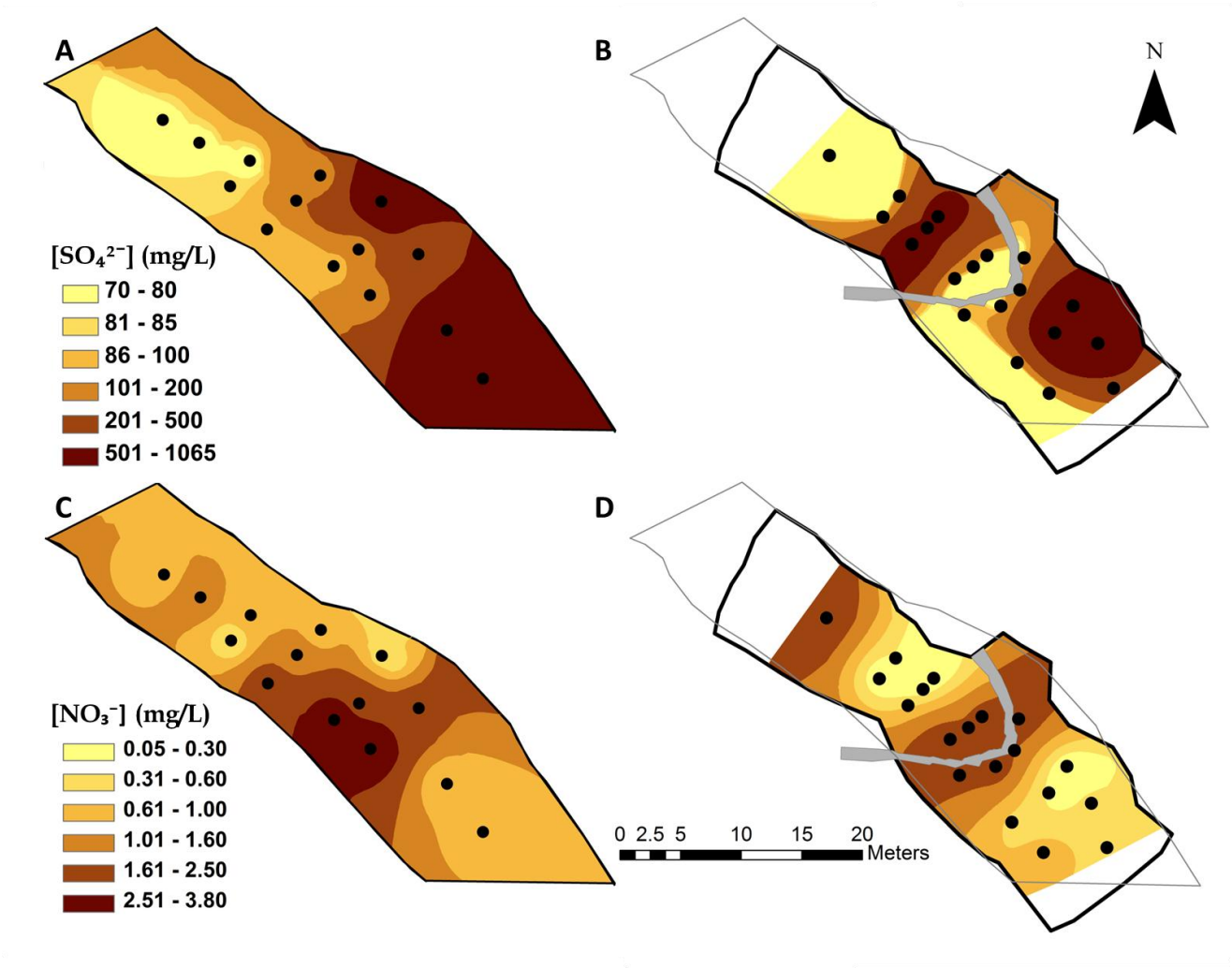

Figure 2.4. Streambed concentrations of (A) sulfate pre-restoration, (B) sulfate post-restoration, (C) nitrate pre-restoration, (D) and nitrate post-restoration, during baseflow conditions. Lighter colors represent lower concentrations and darker colors represent higher concentrations. Contours were interpolated using ArcGIS.

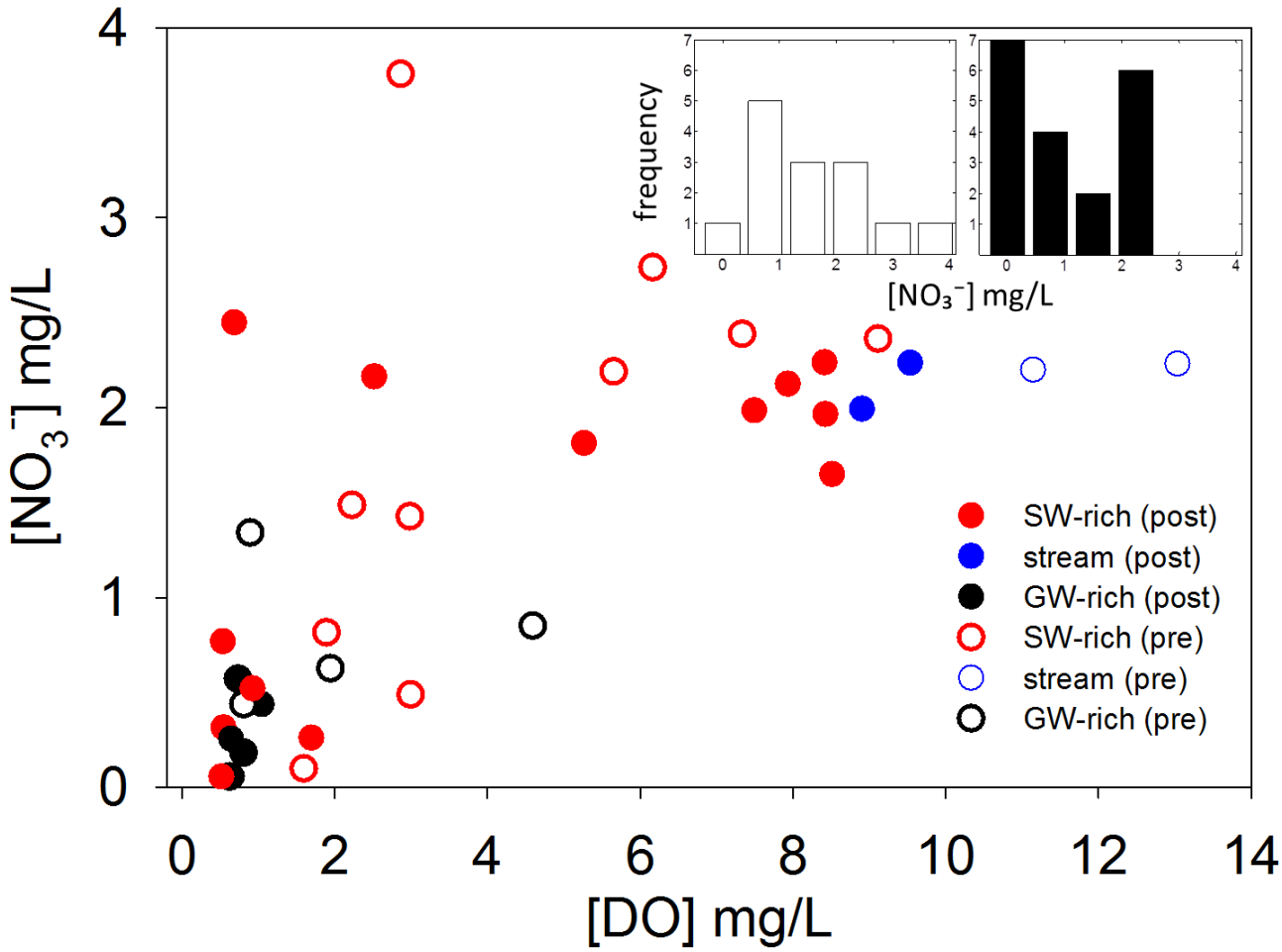

Figure 2.5. Nitrate concentrations versus dissolved oxygen concentrations for pore water and stream water pre- and post- restoration. Open circles represent pre-restoration and filled circles represent post-restoration. Red represents SW-rich streambed sites, blue represents stream water, and black represents GW-rich streambed sites. Inset: Histograms of nitrate concentrations for pre- (white bars) and post- (black bars) restoration.

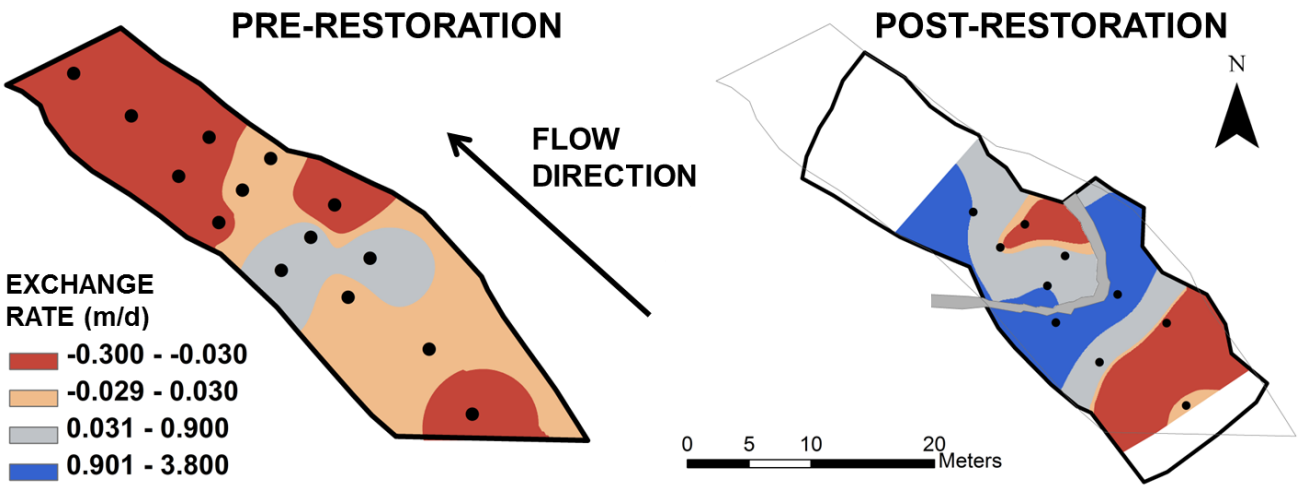

Figure 2.6. Plot of vertical exchange flux (cm/d) across the streambed interface averaged between 2.5 and 5.0 cm depths during baseflow conditions for pre- and post-restoration. Contours were interpolated using ArcGIS. Red indicates upwelling (negative values) and blue indicates downwelling (positive values).

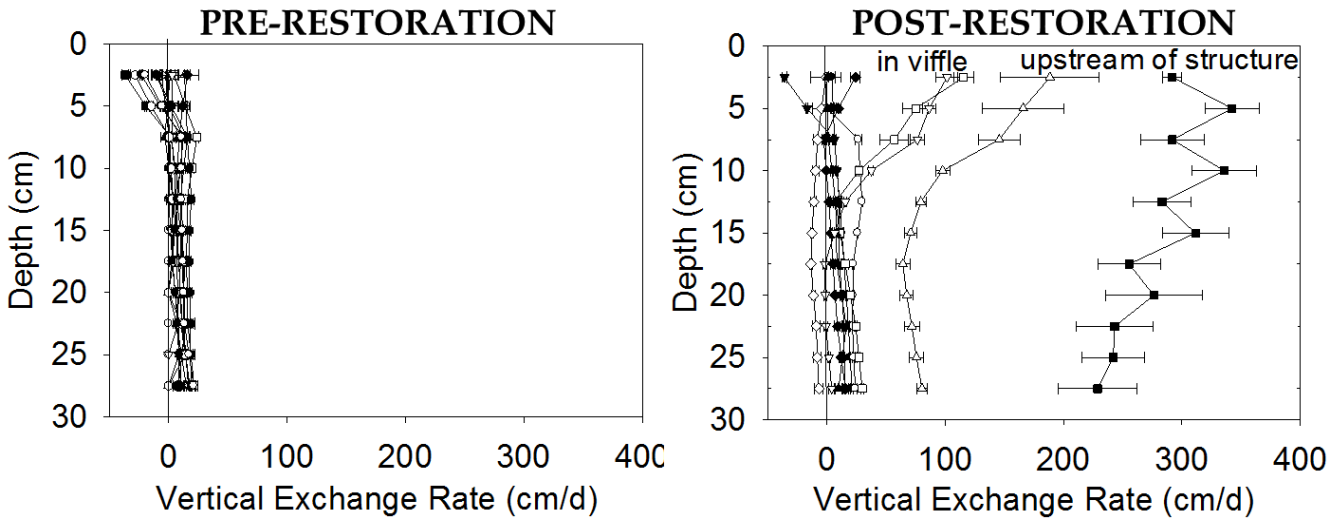

Figure 2.7. Plot of vertical exchange flux (cm/d) across all depths intro the streambed during baseflow conditions for pre- and post-restoration. Positive values indicate downwelling and negative values indicate upwelling. Error bars represent one standard deviation from the calculated mean exchange rate value.

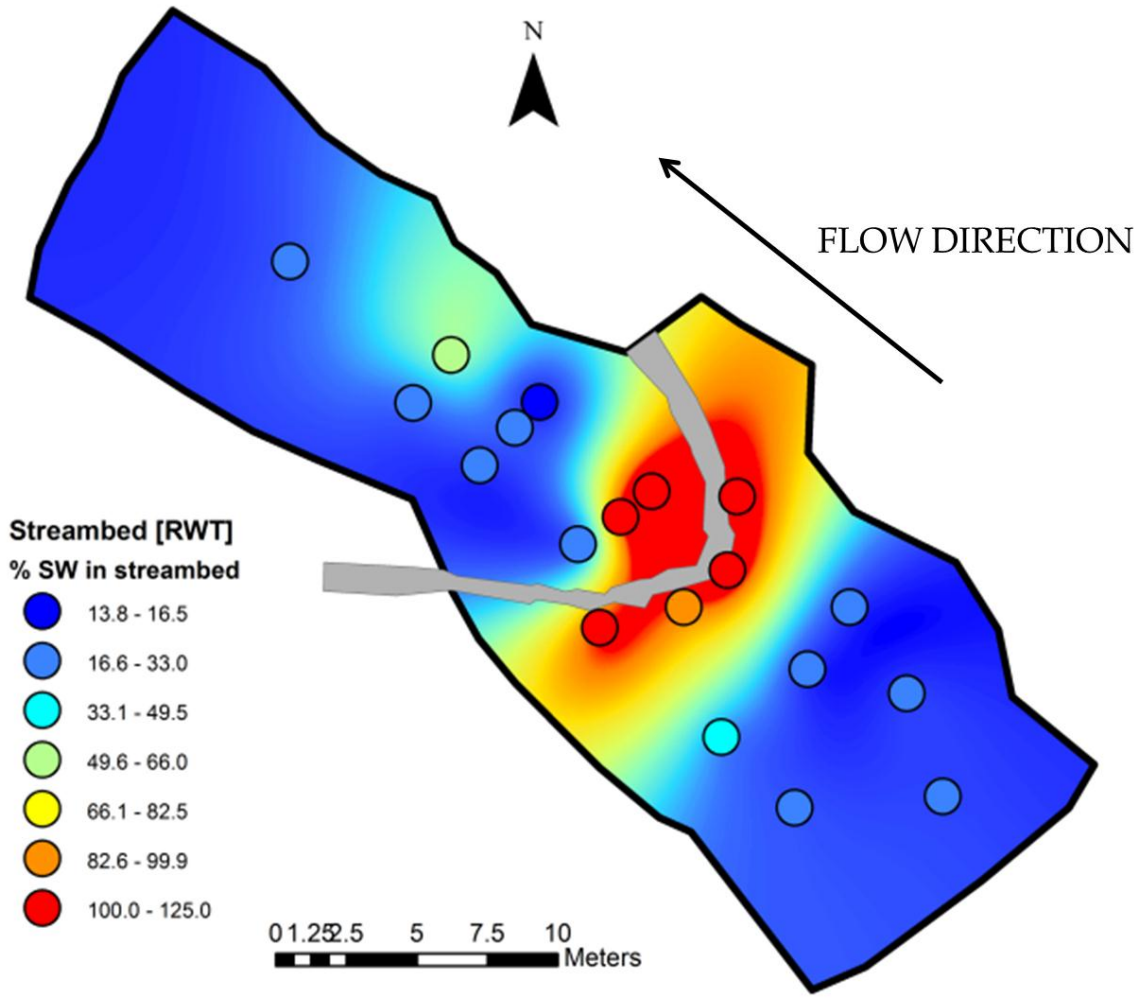

Figure 2.8. Percentage of stream water in streambed during baseflow for post-restoration. Blue colors represent low percentages and red colors represent high percentages. Contours were interpolated using ArcGIS.

References

Arntzen E, Geist DR, Dresel PR. 2006. Effects of fluctuating river flow on groundwater-surface water mixing in the hyporheic zone of a regulated, large cobble bed river. *River Research and Applications* **22**: 937-946.

Bernhardt ES, Palmer MA, Allan JD, Alexander G, Barnas K, Brooks S, Carr J, Clayton S, Dahm C, Follstad-Shah J, Galat D, Gloss S, Goodwin P, Hart D, Hassett B, Jenkinson R, Katz S, Kondolf GM, Lake PS, Lave R, Meyer JL, O'Donnell TK, Pagano L, Powell B, Sudduth E. 2005. Ecology – synthesizing U.S. river restoration efforts. *Science* **308**: 636-637.

Blair JM. 1988. Nutrient release from decomposing foliar litter of three tree species with special reference to calcium, magnesium and potassium dynamics. *Plant and Soil* **110**: 49-55.

Boano F, Camporeale C, Revelli R, Ridolfi L. 2006. Sinuosity-driven hyporheic exchange in meandering rivers. *Geophysical Research Letters* **33**: L18406, doi:10.1029/2006GL027630.

Boano F, Revelli R, Ridolfi L. 2007. Bedform-induced hyporheic exchange with unsteady flows. *Advances in Water Resources* **30**: 148-156.

Boano F, Revelli R, Ridolfi L. 2008. Reduction of the hyporheic zone volume due to the stream-aquifer interaction. *Geophysical Research Letters* **35**: L09401.

Boano F, Revelli R, Ridolfi L. 2010. Effect of streamflow stochasticity on bedform-driven hyporheic exchange. *Advances in Water Resources* **33**: 1367-1374.

Boulton AJ, Findlay S, Marmonier P, Stanley EH, Valett HM. 1998. The functional significance of the hyporheic zone in streams and rivers. *Annual Review of Ecology and Systematics* **29**: 59-81.

Boulton AJ. 2007. Hyporheic rehabilitation in rivers: restoring vertical connectivity. *Freshwater Biology* **52**: 632-650.

Brunke M, Gonser, T. 1997. The ecological significance of exchange processes between rivers and groundwater. *Freshwater Biology* **37**: 1-33.

Briggs MA, Lautz LK, McKenzie JM, Gordon RP, Hare D. 2012. Using high-resolution distributed temperature sensing to quantify spatial and temporal variability in vertical hyporheic flux. *Water Resources Research* **48**: W02527, doi:10.1029/2011WR011227

Cardenas MB, Wilson JL. 2007. Dunes, turbulent eddies, and interfacial exchange with permeable sediments. *Water Resources Research* **43**, doi:10.1029/2008WR007442.

Cardenas MB, Wilson JL. 2007. Exchange across a sediment–water interface with ambient groundwater discharge. *Journal of Hydrology* **346**: 69-80 http://dx.doi.org/10.1016/j.jhydrol.2007.08.019

Conant BJ. 2004. Delineating and quantifying ground water discharge zones using streambed temperatures. *Ground water* **42**: 243-257.

Conant BJ, Cherry A, Gillham RW. 2007. A PCE groundwater plume discharging to a river: Influence of the streambed and near-river zone on contaminant distributions. *Contaminant Hydrology* **73**: 249-279.

Creed IF, Band LE. 1998. Export of nitrogen from catchments within a temperate forest: Evidence for a unifying mechanism regulated by variable source area dynamics. *Water Resources Research* **34**: 3105-3120. doi:10.1029/98WR0192.

Crispell JK, Endreny TA. 2009. Hyporheic exchange flow around constructed in-channel structures and implications for restoration design. *Hydrological Processes* **23**: 1158-1168. doi:10.1002/Hyp.72.30.

D'Angelo DJ, Webster JR, Gregory SV, Meyer JL. 1993. Transient Storage in Appalachian and Cascade Mountain Streams as Related to Hydraulic Characteristics. *Journal of the North American Benthological Society* **3**: 223-235.

Daniluk TL, Lautz LK, Gordon RP, Endreny TA. In press. Surface water-groundwater interaction at restored streams and associated reference reaches. *Hydrological Processes* doi:10.1002/hyp.9501

Edler C. & Dodds W.K. (1992) Characterization of a groundwater community dominated by Caecidotea tridentata (Isopoda). In: Proceedings of the First International Conference on Ground

Water Ecology (Eds J.A. Stanford & J.J. Simons), pp. 91–99, American Water Resources Association, Bethesda, MD, U.S.A.

Elliott AH, Brooks NH. 1997. Transfer of non-sorbing solutes to a streambed with bed forms: Theory. *Water Resources Research* **33**: 123-136.

Fanelli RM, Lautz LK. 2008. Patterns of water, heat, and solute flux through streambeds around small dams. *Ground water* **46**: 671-687.

Findlay, S. 1995. Importance of surface-subsurface exchange in stream ecosystems- The hyporheic zone. *Limnol. Oceanogr*. **40**: 159-164.

Francis BA, Francis LK, Cardenas MB. 2010. Water table dynamics and groundwater–surface water interaction during filling and draining of a large fluvial island due to dam-induced river stage fluctuations. *Water Resources Research* **46**: W07513, doi:10.1029/2009WR008694.

Fritz BG, Arntzen EV. 2007. Effect of Rapidly Changing River Stage on Uranium Flux through the Hyporheic Zone. *Ground water* **45:** 753–760.

Gerecht KE, Cardenas MB, Guswa AJ, Sawyer AH, Nowinski JD, Swanson TE. 2011. Dynamics of hyporheic flow and heat transport across a bed-to-bank continuum in a large regulated river. *Water Resources Research* **47**: W03524, doi:10.1029/2010WR009794.

Gibert J, Dole-Olivier MJ, Marmonier P, Vervier P. 1990. Surface water–groundwater ecotones. In: The Ecology and Management of Aquatic-Terrestrial Ecotones (Eds R.J. Naiman & H. De´camps), pp. 199– 226, UNESCO, Paris and Parthenon Publishers, Carnforth.

Gibert J, Stanford JA, Dole-Olivier MJ, Ward JV. 1994. Basic attributes of groundwater ecosystems and prospects for research. In: Groundwater Ecology (Eds J. Gibert, D.L. Danielopol & J.A. Stanford), pp. 7–40, Academic Press, San Diego.

Gooseff MN. 2010. Defining hyporheic zones – Advancing our conceptual and operational definitions of where stream water and groundwater meet. *Geography Compass* **4**: 945-955.

Gordon RP, Lautz LK, Briggs MA, McKenzie JM. 2012. Automated calculation of vertical pore-water flux from field temperature time series using the VFLUX method and computer program. *Journal of Hydrology* **420-421:** 142-158.

Gordon, RP, Lautz LK**,** Daniluk TL. In press. Spatial patterns of hyporheic exchange and biogeochemical cycling around cross-vane restoration structures: The role of the hyporheic zone and implications for stream restoration design. Water Resources Research.

Guggenmos MR, Daughney CJ, Jackson BM, Morgenstern U. 2011. Regional-scale identification of groundwater-surface water interaction using hydrochemistry and multivariate statistical methods, Wairarapa Valley, New Zealand. *Hydrology and Earth Systems Science Discussion* **8:** 6443–6487 doi:10.5194/hessd-8-6443-2011.

Haack SK, Bekins BB. 2000. Microbial populations in contaminant plumes. *Hydrogeol J* **8**:63-76.

Hakenkamp CC, Morin A, Strayer DL. 2002. The functional importance of freshwater meiofauna. In: Freshwater Meiofauna: Biology and Ecology (Eds S.D. Rundle, A.L. Robertson & J.M. Schmid-Araya), pp. 321–335, Backhuys, Leiden, The Netherlands.

Hancock PJ, Boulton AJ, Humphreys WF. 2005. The aquifer and its hyporheic zone: ecological aspects of hydrogeology. *Hydrogeological Journal* **13**: 98–111.

Hart DR, Mulholland PJ, Marzolf ER, DeAngelis DL, Hendricks SP. 1999. Relationships between hydraulic parameters in a small stream under varying flow and seasonal conditions. *Hydrological Processes* **13**: 1497– 1510.

Harvey JW, Bencala KE. 1993. The effect of streambed topography on surface-subsurface water interactions in mountain catchments. *Water Resources Research* **29**: 89-98.

Harvey JW, Wagner BJ, Bencala KE. 1996. Evaluating the reliability of the stream tracer approach to characterize stream-subsurface water exchange. *Water Resources Research **32***: 2441-2451.

Harvey JW, Wagner BJ. 2000. Quantifying hydrologic interactions between streams and their subsurface hyporheic zones. In *Streams and Ground Waters*, Jones JB, Mulholland PJ (eds). Academic Press: San Diego, CA; 4-41.

Hatch CE, Fisher AT, Revenaugh JS, Constantz K, Ruehl C. 2006. Quantifying surface water-groundwater interactions using time series analysis of streambed thermal records: Method development. *Water Resources Research* **42**: W10410. Doi: 10.1029/2005WR004787.

Harvey JW, Bencala KE. 1993. The effect of streambed topography on surface-subsurface water exchange in mountain catchments. *Water Resources Research* **29**: 89-98.

Hayashi M, Rosenberry DO. 2002. Effects of ground water exchange on the hydrology and ecology of surface water. *Ground Water* **40**: 309-316, doi:10.1111/j.1745-6584.2002.tb02659.x.

Hendricks SP. 1996. Bacterial biomass, activity, and production within the hyporheic zone of a northtemperate stream. *Archiv fu¨ r Hydrobiologie* **136:** 467–487.

Hester ET, Doyle MW. 2008. In-stream geomorphic structures as drivers of hyporheic exchange. *Water Resources Research* **44**: W03417, doi:10.1029/2006WR005810.

Hester ET, Gooseff MN. 2010. Moving beyond the banks: hyporheic restoration is fundamental to restoring ecological services and functions of streams. *Environmental Science and Technology* **44**: 1521-1526.

Hester ET, Gooseff MN. 2011. Hyporheic restoration in streams and rivers, in *Stream Restoration in Dynamic Fluvial Systems: Scientific Approaches, Analyses, and Tools*, pp. 167-187, AGU, Washington, DC.

Hey, RD. 2006. Fluvial geomorphological methodology for natural stable channel design, *J. Am. Water Resourc. Assoc.*, **42**: 357-374.

Hinton MJ, Schiff SL, English MC. 1997. The significant of storms for the concentration and export of dissolved organic carbon from two Precambrian Shield catchments. *Biogeochemistry* **36**: 67-88.

Inamdar SP, Christopher SF, Mitchell MJ. 2004. Export mechanisms for dissolved organic carbon and nitrate during summer storm events in a glaciated forested catchment in New York, USA. *Hydrological Processes* **18**: 2651-2661.

Kasahara T, Hill AR. 2006. Hyporheic exchange flows induced by constructed riffles and steps in lowland streams in southern Ontario, Canada. *Hydrological Processes* **20:** 4287-4305.

Kasahara T, Hill AR. 2006. Effects of riffle-step restoration on hyporheic chemistry in N-rich lowland streams. *Canadian Journal of Fisheries and Aquatic Sciences* **63**: 120-133.

Kasahara, T, Datry T, Mutz M, Boulton AJ. 2009. Treating causes not symptoms: Restoration of surface-groundwater interactions in rivers. *Marine and Freshwater Research* **60**: 976-981.

Kasahara T, Wondzell SM. 2003. Geomorphic controls on hyporheic exchange flow in mountain streams. *Water Resources Research* **39**: 1005, doi: 10.1029/2002WR001386.

Kilpatrick FA, Cobb ED. 1985. Measurement of discharge using tracers: U.S. Geological Survey Techniques of Water-Resources Investigations. Book 3 Chap. A16, 52 p.

Knust AE, Warwick JJ. 2009. Using a fluctuating tracer to estimate hyporheic exchange in restored and unrestored reaches of the Truckee River, Nevada, USA. *Hydrological Processes* **23**: 1119-1130.

Lautz LK, Fanelli RM. 2008. Seasonal biogeochemical hotspots in the streambed around restoration structures. *Biogeochemistry* **91**: 85-104.

Lautz LK, Ribaudo RE. 2012. Scaling up point-in-space heat tracing of seepage flux using bed temperatures as a quantitative proxy. *Hydrogeology Journal* **20:**1223-1238. doi: 10.1007/s10040-012-0870-2

Lave, R. 2009. The controversy over natural channel design: Substantive explanations and potential avenues for resolution. *J. Am. Water Resour. Assoc*. **45**: 1519-1532.

Lewandowski J, Lischeid G, Nutzmann G. 2009. Drivers of water level fluctuations and hydrological exchange between groundwater and surface water at the lowland River Spree (Germany): field study and statistical Analyses. *Hydrological Processes* **23**: 2117-2128. doi: 10.1002/hyp.7277

Malcolm IA, Soulsby C, Youngson AF. 2006. High frequency logging technologies reveal state-dependent hyporheic process dynamics: implications for hydroecological studies. *Hydrological Processes* doi: 10.1002/hyp.6107.

Malcolm IA, Soulsby C, Youngson AF, Hannah DM, McLaren IS, Thorne A. 2004. Hydrological influences on hyporheic water quality: implications for salmon egg survival. *Hydrological Processes* doi. 10.1002/hyp.140.5.

Marmonier P, Vervier P, Gibert J, Dole-Olivier MJ. 1993. Biodiversity in ground waters. *Trends Ecol. Evol.* **8**: 392-295.

Morrice JA, Valett HM, Dahm CN, Campana ME. 1997. Alluvial characteristics, groundwater-surface water exchange and hydrological retention in headwater streams. *Hydrological Processes* **11**: 253-267

Rosgen, DL. 1994. A classification of natural rivers. *Catena* **22**:169-199.

Rosgen DL. 1998. The Reference Reach – A Blueprint for Natural Channel Design. In Proceedings of ASCE Specialty Conference on Restoration, Denver, Colo.

Rosgen DL.2001. Cross-vane, w-weir, and j-hook vane structures: description, design and application for stream stabilization and river restoration. Proceedings of the Wetlands Engineering and River Restoration Conference. Published by American Society of Civil Engineers: Reno, Nevada, USA. doi:10.1061/40581(2001)72.

Rosgen DL. 2011. Natural channel design: fundamental concepts, assumptions, and methods. In stream Restoration in Dynamic Fluvial Systems: scientific approaches, analyses, and tools, Simon A, Bennett SJ, Castro JM (eds). American Geophysical Union: Washington, DC.

Sawyer AH, Cardenas MB, Bomar A, Mackey M. 2009. Impact of dam operations on hyporheic exchange in the riparian zone of a regulated river. *Hydrological Processes* **23**: 2129-2137.

Shibata H, Sugawara O, Toyoshima H, Wondzell SM, Nakamura F, Kasahara T, Swanson FJ, Sasa K. 2004. Nitrogen dynamics in the hyporheic zone of a forested stream during a small storm, Hokkaido, Japan. *Biogeochemistry* **69**: 83-104.

Smith JJ, Lake PS. 1993. The breakdown of buried and surface-placed leaf litter in an upland stream. *Hydrobiologia* **271**: 141-148.

Stanford JA, Ward JV. 1993. An ecosystem perspective of alluvial rivers: connectivity and the hyporheic corridor. *Journal of the North American Benthological Society* **12**: 48-60.

Storey RG, Howard KWF, Williams DD. 2003. Factors controlling riffle-scale hyporheic exchange flows and their seasonal changes in a gaining stream: A three-dimensional groundwater flow model. *Water Resources Research* **39**: 1034, DOI:10.1029/2002WR001367

Strayer DL. 1994. Limits to biological distributions in groundwater. In: Gibert J, Danielopol DL, Stanford JA (eds) Groundwater ecology. Academic Press, San Diego, 287-313.

Valett HM, Fisher SG, Grimm NB, Camill P. 1994. Vertical Hydrologic Exchange and Ecological Stability of a Desert Stream Ecosystem. *Ecology* **75:** 548-560.

Vervier P, Gibert J, Marmonier P, Dole-Olivier MJ. 1992. A perspective on the permeability of the surface freshwater-groundwater ecotone. *Journal of the North American Benthological Society* **11**: 93-102.

Westhoff MC, Bogaard TA, Savenije HHG. 2011. Quantifying spatial and temporal discharge dynamics of an event in a first order stream, using distributed temperature sensing. *Hydrology and Earth Systems Science* **15:** 1945-1957.

Wondzell SM. 2011. The role of the hyporheic zone across stream networks. *Hydrological Processes* **25**: 3525-3532.

Wondzell SM, Swanson FJ. 1996. Seasonal and storm dynamics of the hyporheic zone of a 4th-rrder mountain stream. *Journal of the North American Benthological Society* **15**: 3-19.

Wroblicky GJ, Campana ME, Valett HM, Dahm CN. 1998. Seasonal variation in surface-subsurface water exchange and lateral hyporheic area of two stream-aquifer systems. *Water Resources* R*esearch* **34**: 317-328.

Zarnetske JP, Haggerty R, Wondzell SM, Baker MA. 2011. Dynamics of nitrate production and removal as a function of residence time in the hyporheic zone. Journal of Geophysical Research DOI:10.1029/2010JG001356.

Zimmer MA, Lautz LK. In press. Temporal and spatial response of hyporheic zone geochemistry to a storm event. *Hydrological Processes.*

Curriculum Vitae

Margaret (Maggie) A. Zimmer

Department of Earth Sciences, 204 Heroy Geology Laboratory
Syracuse University, Syracuse, NY 13244
503-702-1651 mazimm02@syr.edu

EDUCATION

Syracuse University, Syracuse, NY May 2013
M.Sc. Earth Sciences

Oberlin College, Oberlin, Ohio May 2011
B.A., Environmental Studies with minors in Economics and Geology
Highest Honors for a distinguished Senior Thesis

APPOINTMENTS

Research Assistant, Department of Earth Sciences, Syracuse University 2012
Studied spatial and temporal variations of hyporheic geochemistry pre- and post- restoration during storm events. Used ion chromatography and heat tracing techniques in site analysis.

Teaching Assistant, Department of Earth Sciences, Syracuse University 2011-2012
Wrote weekly assignments for the lab portion of assigned course. Taught and lead daily labs.

Research Assistant, Hubbard Brook Experimental Forest, Plymouth, New Hampshire 2010
Continuation of research described below.

NSF REU Intern, Hubbard Brook Experimental Forest, Plymouth, New Hampshire 2009
Implemented six watershed-scale sample surveys to monitor spatial and temporal stream chemistry. Compared results to groundwater chemistry of samples collected from wells I installed in varying soil types.

Research Aide, University of Alaska-Fairbanks, Fairbanks, Alaska 2008
Conducted reach-scale conservative/non-conservative tracer tests to study stream-groundwater interactions and nutrient uptake rates in sub-arctic streams.

NOTABLE AWARDS AND HONORS

NSF Graduate Research Fellowship 2013
NSF Graduate Research Fellowship – Honorable Mention 2012
Outstanding Student Paper Award –AGU Fall Meeting 2011
Geological Society of America Student Research Grant 2011
Sigma Xi Scientific Honor Society 2011

PROFESSIONAL DEVELOPMENT

Founder/organizer, Cross-campus hydrology graduate student support/working group – CAFÉ Hydro, Syracuse University/SUNY ESF 2012-present

Founder/organizer, Cross-campus water listserv and website – waternews@syr.edu, Syracuse University/SUNY ESF 2012-present

Organizer, Departmental Graduate Student Seminar, Syracuse University 2011-present

Board member, Oberlin College Environmental Studies Alumni Association 2010-present

Student representative, Oberlin College Environmental Studies Department 2009-2011

PUBLICATIONS

Zimmer MA, Lautz LK. In prep. Pre- and post- restoration assessment of stream-ground water interactions: impacts on hydrological and chemical heterogeneity in the hyporheic zone. *Freshwater Science.* Invited Special Issue. DOI: 10.1002/hyp.9778

Zimmer MA, Lautz LK. 2013. Temporal and spatial response of hyporheic zone geochemistry to a storm event. *Hydrological Processes*. DOI: 10.1002/hyp.9778

Zimmer MA, Bailey SW, McGuire KJ, Bullen TD. 2012. Fine scale variations of surface water chemistry in an ephemeral to perennial drainage network. *Hydrological Processes*. DOI:10.1002/hyp.9449

SELECT PRESENTATIONS AND PUBLISHED ABSTRACTS

Zimmer MA, Bailey SW, McGuire KJ, Bullen TD. 2013. Variation in surface water chemistry at two scales of observation at the Hubbard Brook Experimental Forest. US-Japan Joint Seminar on Catchment Hydrology, Honolulu, HI, Mar 4-7.

Zimmer MA, Lautz LK. 2012. Temporal and spatial effects of a storm event on hyporheic zone geochemistry, Abstract H11D-1204 presented at 2012 Fall Meeting, AGU, San Francisco, CA, 3-7.

Ward AS, Robinson J, Endreny TA, Cullin J, Smidt S, Lautz L, **Zimmer MA.** 2012. Do stream restoration structures create hyporheic zones that are comparable to those at natural features? Abstract H12B-06 presented at 2012 Fall Meeting, AGU, San Francisco, CA, Dec. 3-7.

Zimmer, MA. 2012. What can spatial and temporal stream chemistry tell us about the main chemical drivers and water sources at Hubbard Brook Experimental Forest? Lunch and Learn Seminar. US Geological Survey, Troy, NY, Sept. 24, 2012.
Also presented at Natural Science Seminar, Le Moyne College, Syracuse, NY, Oct. 12, 2012.

Zimmer MA, Bailey SW, McGuire, KJ. 2011. Fine scale variations of surface water chemistry in an ephemeral to perennial drainage network in the Hubbard Brook Experimental Forest, NH, USA, Abstract H53F-1490 presented at 2011 Fall Meeting, AGU, San Francisco, CA, 5-9 Dec.

Bullen TD, Bailey SW McGuire KJ, **Zimmer MA,** Ross DS. 2011. Determining solute sources and water flowpaths in a forested headwater catchment: advances with the Ca-Sr-Ba multi-tracer, Abstract EP51F-07 presented at 2011 Fall Meeting, AGU, San Francisco, CA., 5-9 Dec.

Zimmer MA. Fine scale variations of surface water chemistry in an ephemeral to perennial drainage network. Oral (**Invited**). Western Ecology Division at EPA, Corvallis, OR. Nov. 2011.

Zimmer MA, Bailey SW, McGuire KJ. 2011. Fine scale variations of surface water chemistry in an ephemeral to perennial drainage network in the Hubbard Brook Experimental Forest, NH, USA. GSA 43(5) 472. Fall Meeting Suppl., 9-12 Oct.

Zimmer MA., Bailey SW, McGuire KJ, Bullen TD. 2011. Hydropedology reveals spatial distribution of processes controlling stream solute export: clues from spatial and temporal variation in surface water chemistry. Gordon Research Conference on Catchment Science, July 10-15, Lewiston, ME.

Bullen TD, Bailey SW, **Zimmer MA**, McGuire KJ, Bourgault R, Ross D. 2011. Hydropedology reveals spatial distribution of processes controlling stream solute sources: chemical and isotopic clues. Gordon Research Conference on Catchment Science, July 10-15, Lewiston, ME.

Zimmer MA, Bailey SW, McGuire KJ, Bullen TD. 2010. Determining surface water sources using spatial and temporal variation in stream chemistry in a headwater catchment. Abstract B43C-0469 presented at 2010 Fall Meeting, AGU, San Francisco, CA, 13-17 Dec.

Bullen TD, Bailey SW, McGuire KJ, Brousseau P, Ross DS, Bourgault R, **Zimmer MA**. 2010. Understanding metal sources and transport processes in watersheds: a hydropedologic approach (**Invited**). Abstract B23K-06 presented at 2010 Fall Meeting, AGU, San Francisco, CA, 13-17 Dec.

TEACHING EXPERIENCE

Invited Guest Lecture – Watershed Hydrology, SUNY ESF	2013
Volcanoes and Earthquakes Teaching Assistant, Dept. of Earth Sciences, SU	2012
Oceanography Teaching Assistant, Dept. of Earth Sciences, Syracuse University	2011
Introductory Soil Science Course Lecturer, Geology Dept., Oberlin College	2010